Journal of Medicinal Chemistry

pubs.acs.org/jmc

Article

Hydrogel-Encapsulated Biofilm Inhibitors Abrogate the Cariogenic Activity of *Streptococcus mutans*

Parmanand Ahirwar,[○] Veronika Kozlovskaya,[○] Bhavitavya Nijampatnam, Edwin M. Rojas, Piyasuda Pukkanasut, Daniel Inman, Maksim Dolmat, Anna C. Law, Norbert Schormann, Champion Deivanayagam, Gregory J. Harber, Suzanne M. Michalek, Hui Wu,* Eugenia Kharlampieva,* and Sadanandan E. Velu*

Cite This: *J. Med. Chem.* 2023, 66, 7909−7925

Read Online

ACCESS | Metrics & More | Article Recommendations | Supporting Information

ABSTRACT: We designed and synthesized analogues of a previously identified biofilm inhibitor **IIIC5** to improve solubility, retain inhibitory activities, and to facilitate encapsulation into pH-responsive hydrogel microparticles. The optimized lead compound **HA5** showed improved solubility of 120.09 μg/mL, inhibited *Streptococcus mutans* biofilm with an IC_{50} value of 6.42 μM, and did not affect the growth of oral commensal species up to a 15-fold higher concentration. The cocrystal structure of **HA5** with GtfB catalytic domain determined at 2.35 Å resolution revealed its active site interactions. The ability of **HA5** to inhibit *S. mutans* Gtfs and to reduce glucan production has been demonstrated. The hydrogel-encapsulated biofilm inhibitor (**HEBI**), generated by encapsulating **HA5** in hydrogel, selectively inhibited *S. mutans* biofilms like **HA5**. Treatment of *S. mutans*-infected rats with **HA5** or **HEBI** resulted in a significant reduction in buccal, sulcal, and proximal dental caries compared to untreated, infected rats.

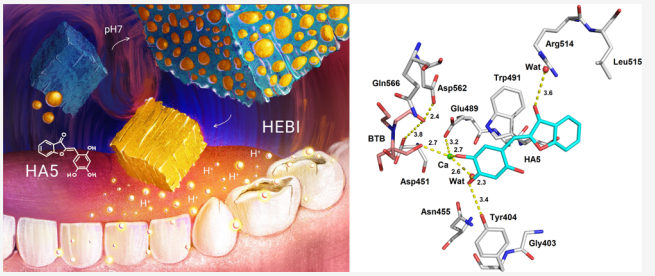

INTRODUCTION

Majority of the tooth- and gum-related diseases are associated with bacterial infections. Among these, dental caries (tooth decay) is a ubiquitous disease that affects most of the human population. Dental caries is a multifactorial disease that causes localized destruction of susceptible dental tissues.[1] Dental caries is identified as the most prevalent disease worldwide in a recent Lancet study of global burden of 328 major diseases.[2] Despite its general classification as a "life-style-related" disease, dental caries poses a significant challenge as it results in tooth loss, infection, and in some cases, even death by sepsis.[3,4]

Current treatments for this disease have severe limitations. The conventional oral hygiene practices such as brushing or mouthwashes are not highly effective due to the rapid recolonization of bacteria.[5] Fluoride sealants and varnishes are commonly used to prevent dental caries in children.[6] While there is a general consensus on the safety of fluoride treatments,[7] their high fluoride content (1−5%) and potential neurotoxic effects are a concern.[8] The antimicrobial agents used in mouthwashes such as chlorhexidine, xylitol, silver diamine fluoride, and delmopinol lack selectivity, affecting both pathogenic and commensal beneficial species alike giving rise to undesired side effects such as vomiting, diarrhea, addiction, or teeth discoloration.[9] In addition, the biofilm nature of cariogenic bacteria makes it resistant to traditional antimicrobial treatments.[10] A few preventive and therapeutic strategies are under investigation by targeting different virulent determinants of *Streptococcus mutans*.[11] However, small molecules derived from natural products that possess antibacterial activities and anti-biofilm properties are randomly identified inhibitors that lack selectivity toward pathogenic biofilms and the *in vivo* applications of these inhibitors are unclear.[12]

Dental plaque consists of more than 700 bacterial species living in complex communities called biofilms.[4] It is initiated by the attachment of commensal streptococci such as *Streptococcus sanguinis* and *Streptococcus gordonii* to the saliva-coated tooth surface, which then engage in developing intra- and interspecies bacterial interactions.[13] Under disease conditions, the delicate balance between commensal and pathogenic members of the plaque bacteria is disturbed, leading to an overgrowth of pathogenic species.[14] *S. mutans* has been implicated as the major etiological agent in the initiation and propagation of this disease.[15] The formation of tenacious biofilms is the hallmark of *S. mutans*-induced cariogenesis. Therefore, the studies aimed at developing dental caries

Received: February 15, 2023
Published: June 7, 2023

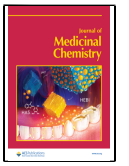

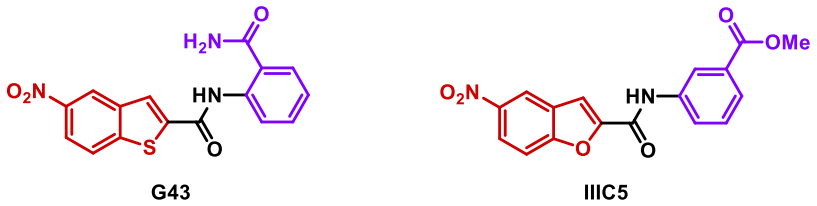

Figure 1. Chemical structures of **G43** and **IIIC5**.

treatments should focus on identifying selective inhibitors of biofilms that do not affect the growth of oral commensal bacteria.

Major virulence factors of *S. mutans* that significantly contribute to its ability to form cariogenic biofilm are its extracellular glucosyl transferases (Gtfs).[16] Most strains of *S. mutans* harbor three distinct *gtf* genes expressing different Gtf activities. The genes *gtfB* and *gtfD* produce GtfB and GtfD enzymes, respectively, and synthesize predominantly water-insoluble and soluble glucans[17] correspondingly, while *gtfC* encodes for GtfC, an enzyme that synthesizes both water-insoluble and soluble glucans.[18] *S. mutans* GtfB and GtfC are essential for glucan synthesis, bacterial colonization, and cariogenesis. Therefore, small-molecule inhibitors of *S. mutans* Gtfs[19−21] have potential application in treating and preventing dental caries.

Many anti-biofilm agents display poor efficacy within the oral cavity due to poor solubility, inability to penetrate biofilms, and lack of ability to retain in the locally infected areas. Given these challenges, antibacterial nanoparticles have generated recent interest due to their potential applications in anticaries research. Examples of these are silver nanoparticles in the prevention of dental caries,[22] farnesol and myricetin coloaded nanoparticles to inhibit biofilms,[23] pH-responsive materials to deliver farnesol,[24] porous silicon microparticles to mitigate cariogenic biofilms,[25] ferumoxytol nanoparticles,[26] poly(ethylenimine),[27] and chitosan nanoparticles[28] with strong antibacterial activity against *S. mutans*. Several nanosystems for controlled release of anticaries drugs have also been explored including mesoporous silica nanoparticle,[29] liposome,[30] halloysite nanotube,[31] polyamidoamine,[32] and dextran-coated iron oxide nanoparticles (nanozymes).[33] Despite the flurry of these recent studies, none of these agents have translated for clinical use as their *in vivo* efficacies are either modest or not proven.

Under physiological conditions, the human salivary system maintains a healthy pH range of 6.0−7.5 in the oral cavity[34] using three buffer systems: (1) bicarbonate, (2) phosphate, and (3) salivary proteins.[35] A salivary pH below 5.5 is potentially harmful to the hard and soft tissues in the oral cavity.[36] Under pathogenic oral conditions, biofilms ferment dietary carbohydrates to produce acidic byproducts such as lactic acid, which decreases the pH and causes demineralization of the tooth enamel.[37] Therefore, a drug that can specifically inhibit the biofilm delivered into the oral cavity in a pH-responsive manner would be highly desirable. Since the pH level in the oral cavity is critical for the demineralization of tooth enamel, our efforts were focused on developing a novel drug delivery system with built-in pH sensitivity for the delivery of biofilm inhibitors as an anticaries treatment.

Our recent studies aimed at developing selective small-molecule inhibitors of *S. mutans* biofilms targeted the *S. mutans*' surface enzymes, Gtfs.[19−21] These studies have resulted in the identification of two potent lead compounds **G43** and **IIIC5** (Figure 1).[19] The goals of the present study were to improve the solubility of the lead biofilm inhibitor **IIIC5** to encapsulate the optimized lead in pH-responsive hydrogel microparticles and to explore its biofilm and growth inhibitory activities *in vitro* and antivirulence activities *in vivo*.

RESULTS AND DISCUSSION

Design and Synthesis of Biofilms Inhibiting Aurone Compounds. Our initial efforts to prepare pH-responsive hydrogel-encapsulated biofilm inhibitors using compound **G43** or **IIIC5** did not yield the expected results due to the low solubility (10−25 μg/mL) of these inhibitors. Therefore, efforts were made to modify the structure of **IIIC5** to improve solubility. Specifically, analogues of **IIIC5** were prepared by substituting the benzofuran ring with a structurally similar aurone ring, removing the nitro, amide, and ester groups, and by introducing multiple hydrophilic OMe or OH groups on the phenyl ring. This study resulted in the identification of several aurone derivatives (**MA1−6** and **HA2−6**, Figure 2), of which the hydroxyaurones were found to have the desired solubility required for hydrogel encapsulation while maintaining the potency and selectivity of biofilm inhibition.

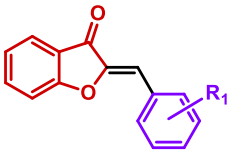

Methoxy aurones (MA)	Hydroxy aurones (HA)
MA1, R_1 = H	
MA2, R_1 = 4-OMe	**HA2**, R_1 = 4-OH
MA3, R_1 = 3,4-di-OMe	**HA3**, R_1 = 3,4-di-OH
MA4, R_1 = 3,5-di-OMe	**HA4**, R_1 = 3,5-di-OH
MA5, R_1 = 2,4,5-tri-OMe	**HA5**, R_1 = 2,4,5-tri-OH
MA6, R_1 = 3,4,5-tri-OMe	**HA6**, R_1 = 3,4,5-tri-OH

Figure 2. Methoxy and hydroxyaurones.

Aurones are a class of organic compounds that are gaining interest in medicinal chemistry due to their biological activities and presence in natural products.[38] Aurone natural products play an important role in the pigmentation of flowers and fruits.[39] Their reported bioactivities range from antifungal activity,[40] antifeedant activity,[41] tyrosinase inhibition,[42] and antioxidant activity.[43] In vitro antimicrobial activities of aurones and chalcones are widely reported.[44] Biosynthetically, aurones are derived from chalcones.[39] Therefore, we took a biomimetic synthetic approach (Scheme 1) to generate a small library of aurones (Figure 2), which includes one aurone derivative with an unsubstituted phenyl ring (**MA1**), five methoxy-substituted aurones (**MA2−6**), and five hydroxy-

https://doi.org/10.1021/acs.jmedchem.3c00272
J. Med. Chem. 2023, 66, 7909−7925

Scheme 1. Synthesis of Substituted Aurones

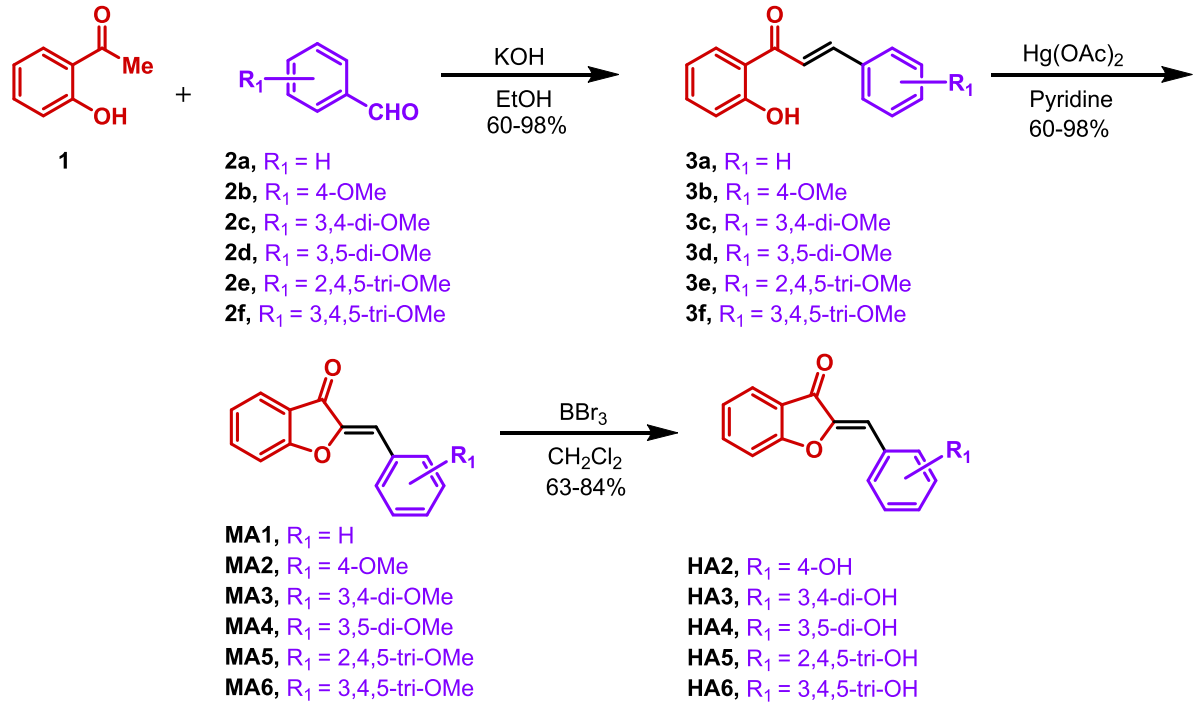

substituted aurones (**HA2−6**). These aurones were prepared from 2-hydroxychalcones (**3a−f**), which in turn were prepared by the Claisen−Schmidt aldol condensation[45] of benzaldehydes (**2a−f**) and 2-hydroxyacetophenone (**1**) in the presence of KOH in ethanol in 37−90% yield. Cyclization of chalcones (**3a−f**) in the presence of $Hg(OAc)_2$ in anhydrous pyridine afforded aurones (**MA1−6**) in 79−100% yield. Methyl groups in methoxyaurones (**MA2−6**) were then removed by treatment with BBr_3 in anhydrous CH_2Cl_2 to afford hydroxyaurones (**HA2−6**) in 80−86% yield.

One of the goals for this study was to improve the solubility of the lead compound, so solubilities of **MA1−6** and **HA2−6** were determined as reported[46,47] (Table 1). As expected, the majority of aurone derivatives had better solubility than the lead compound **IIIC5** (25 μg/mL).[19] Among the aurones, hydroxyaurones were found to be more soluble than methoxyaurones and a trend of increasing solubility was observed with the increase in the number of hydroxy groups on the phenyl ring. The hydroxyaurone **HA5** with the 2,4,5-trihydroxyphenyl ring was found to be the most soluble analogue with a solubility of 120.09 μg/mL. A close analogue **HA6** with a 3,4,5-trihydroxyphenyl ring had the next highest solubility (90.77 μg/mL). The monohydroxyphenyl analogue **HA2** showed the lowest solubility (18.93 μg/mL) among the hydroxyaurones. Methoxyaurones displayed a similar trend of increase in solubility with the increase in the number of methoxy groups. The least soluble methoxyaurone was found to be the monomethoxy analogue **MA2** with the solubility of 16.23 μg/mL. Trimethoxyaurone analogues **MA5** and **MA6** were found to be the most soluble methoxyaurone analogues with the solubilities of 42.36 and 44.68 μg/mL, respectively. The only exception to this trend was the 3,5-dimethoxy analogue **MA4** that showed lower solubility of 18.97 μg/mL compared to 3,4-dimethoxy analogue **MA3** (36.26 μg/mL). The aurone analogues that displayed lower solubility than **IIIC5**[19] are **MA1**, **MA2**, **MA4**, and **HA2**.

Inhibition of *S. mutans* UA159 Planktonic Growth. In order to identify inhibitors of the cariogenic biofilm without affecting the growth of oral bacteria, we first evaluated the effects of compounds **3a−e**, **MA1−6**, and **HA2−6** on *S. mutans* planktonic growth at a single concentration of 50 μM.[48] No significant inhibition of planktonic growth was observed between the control group and treated groups for all chalcone derivatives, **3a−f** (Figure 3A). Methoxyaurones **MA2−6** were found to be slightly more bactericidal than chalcones showing 25−40% planktonic growth inhibition (Figure 3B). The aurone analogue with an unsubstituted phenyl ring (**MA1**) showed the highest bactericidal activity with 80% inhibition of the planktonic growth. Some of the hydroxyaurones were more bactericidal than chalcones and methoxyaurones with **HA2**, **HA3**, and **HA4** showing 60, 40, and 30% inhibition, respectively. Two hydroxyaurones **HA5** and **HA6** did not inhibit the planktonic growth of *S. mutans* at 50 μM and appeared to be promising lead compounds (Figure 3C) for further evaluation.

Inhibition of *S. mutans* UA159 Biofilms. Initial screening of compounds **3a−f**, **MA1−6**, and **HA2−6** in a single species *S. mutans* biofilm assay was carried out at a single treatment dose of 50 μM. Members of all three series of compounds were effective in inhibiting biofilms with hydroxyaurones exhibiting most pronounced activity compared to methoxyaurones and chalcones (Figure 4). More importantly, all compounds showed varying degrees of selectivity toward inhibition of the biofilm as opposed to growth. Chalcones **3a−f** were generally less active compared to aurones (Figure 4A). The most active chalcone derivative **3f** exhibited 40% biofilm inhibition and no growth inhibition at 50 μM. The most potent methoxyaurone **MA5** exhibited 60% biofilm inhibition (Figure 4B). However, this compound also inhibited 30% of bacterial growth at 50 μM, making it a less selective biofilm inhibitor. The other methoxyaurones **MA1**, **MA2**, **MA4**, and **MA6** were relatively less active displaying

https://doi.org/10.1021/acs.jmedchem.3c00272
J. Med. Chem. 2023, 66, 7909−7925

Table 1. Reaction Yields, Solubility, and Biofilm Inhibition Profiles of 3a−f, MA1−6, and HA2−6[e]

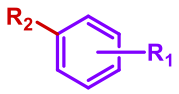

Compd No	R_2 Group	R_1 Group	Yield[a] (%)	Solubility[b] (μg/mL)	Biofilm IC_{50}[c] (μM)
IIIC5[19]		NA	NA	25 ± 0.00	2.70 ± 0.09
3a	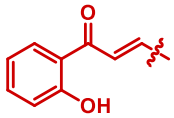	H	62	-[d]	>300[e]
3b		4-OMe	37	-[d]	>300[e]
3c		3,4-di-OMe	53	-[d]	>300[e]
3d		3,5-di-OMe	78	-[d]	>300[e]
3e		2,4,5-tri-OMe	90	-[d]	>300[e]
3f		3,4,5-tri-OMe	85	-[d]	180.80 ± 0.65
MA1		H	78	8.51 ± 2.00	33.61 ± 0.53
MA2	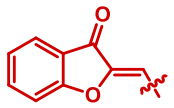	4-OMe	93	16.23 ± 0.41	107.80 ± 0.65
MA3		3,4-di-OMe	100	36.26 ± 1.56	49.40 ± 4.79
MA4		3,5-di-OMe	89	18.97 ± 2.33	>300[e]
MA5		2,4,5-tri-OMe	99	42.36 ± 2.86	52.81 ± 7.42
MA6		3,4,5-tri-OMe	89	44.68 ± 0.87	>300[e]
HA2	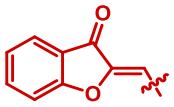	4-OH	89	18.93 ± 1.41	18.79 ± 2.36
HA3		3,4-di-OH	92	81.56 ± 2.90	30.67 ± 2.28
HA4		3,5-di-OH	80	76.50 ± 0.57	94.22 ± 2.18
HA5		2,4,5-tri-OH	83	120.09 ± 1.73	6.42 ± 0.61
HA6		3,4,5-tri-OH	86	90.77 ± 0.48	18.92 ± 0.39
G43[21]	NA	NA	NA	NA	6.28 ± 0.58
Salicylic acid[47]	NA	NA	NA	1880 ± 30	NA

[a]Isolated yield and the compounds are fully characterized with ^{1}H NMR, ^{13}C NMR, and HRMS. [b]Solubility in water containing 1% DMSO determined by UV spectroscopy. [c]*S. mutans* UA159 was coincubated with the compounds at various concentrations and biofilm formation was measured at OD_{562} using an established crystal violet protocol.[48] IC_{50} values represent the mean ± standard error of the mean (SEM) from three independent experiments. [d]Not determined. [e]Highest concentration tested.

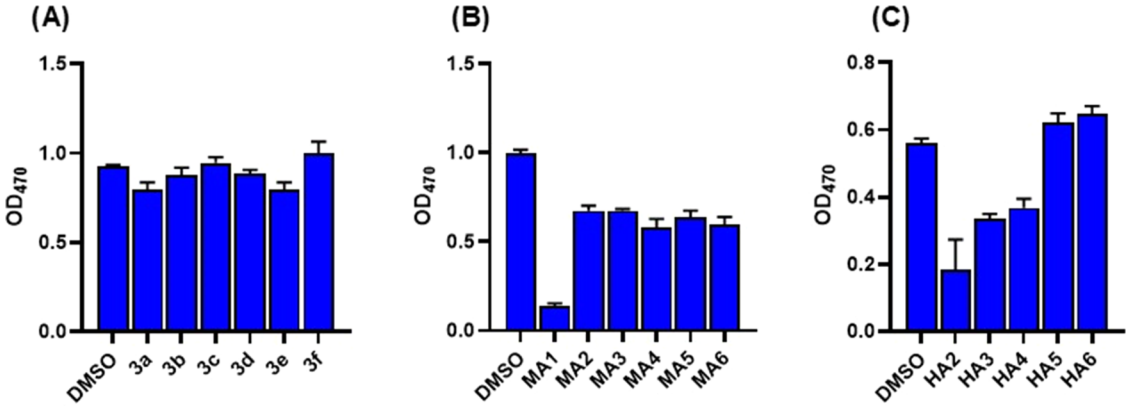

Figure 3. Planktonic growth inhibitory activities of chalcones (**3a−f**), methoxyaurones (**MA1−6**), and hydroxyaurones (**HA2−6**). (A) *S. mutans* UA159 were coincubated with 50 μM chalcones **3a−f** and the planktonic growth was measured at OD_{470}. (B) *S. mutans* UA159 were coincubated with 50 μM methoxyaurones **MA1−6** and the planktonic growth was measured at OD_{470}. (C) *S. mutans* UA159 were coincubated with 50 μM hydroxyaurones **HA2−6** and the planktonic growth was measured at OD_{470}. Each experiment was repeated three times with triplicate microwells for each compound. Statistical significance was tested with one-way ANOVA. $p < 0.0001$.

only 20−40% biofilm inhibition, while **MA3** was inactive at this dose. Overall, hydroxyaurones were better biofilm inhibitors than chalcones and methoxyaurones with derivatives **HA2**, **HA5**, and **HA6** showing more than 95% inhibition and **HA3** showing about 80% inhibition of biofilms (Figure 4C). Among the most active hydroxyaurones, 4-hydroxy analogue **HA2** inhibited bacterial growth by 70% at the treated dose, making it a less selective biofilm inhibitor (Figure 3C). The 3,5-dihydroxyaurone analogue **HA4** did not show significant biofilm inhibition. The 2,4,5-trihydroxy and 3,4,5-trihydroxy

https://doi.org/10.1021/acs.jmedchem.3c00272
J. Med. Chem. 2023, 66, 7909−7925

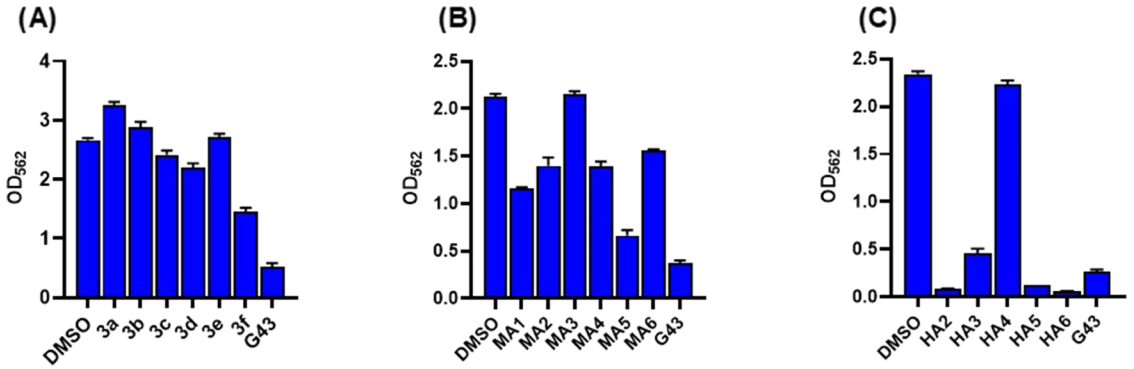

Figure 4. Biofilm inhibitory activities of chalcones (**3a−f**), methoxyaurones (**MA1−6**) and hydroxyaurones (**HA2−6**). (A) *S. mutans* UA159 were coincubated with 50 μM chalcones **3a−f**, and biofilm formation was measured at OD_{562} using the crystal violet protocol. (B) *S. mutans* UA159 were coincubated with 50 μM methoxyaurones **MA1−6**, and biofilm formation was measured at OD_{562} using the crystal violet protocol. (C) *S. mutans* UA159 were coincubated with 50 μM hydroxyaurones **HA2−6**, and biofilm formation was measured at OD_{562} using the crystal violet protocol. Each experiment was repeated three times with triplicate microwells for each compound. Statistical significance was tested with one-way ANOVA. $p < 0.0001$.

analogues **HA5** and **HA6**, respectively, were found to be the most active hydroxyaurone analogues with more than 95% biofilm inhibition and no effect on growth at 50 μM, making them the most active and selective biofilm inhibitors from this screening (Figure 4C).

Inhibition of Commensal Streptococci Biofilms by Hydroxyaurones. To determine the selectivity of hydroxyaurones (**HA2−6**) toward *S. mutans* biofilm formation over the biofilms of commensal species, we evaluated effects of these compounds on the biofilm formation by two oral commensal Streptococci bacteria: *S. gordonii* and *S. sanguinis*. At 50 μM concentration, *S. gordonii* biofilm formation was inhibited by 40−60% (Figure 5A), while *S. sanguinis* biofilm

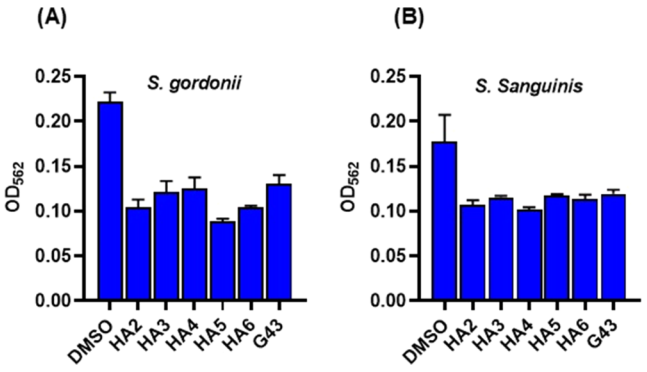

Figure 5. Inhibitory activities of hydroxyaurones (**HA2−6**) against commensal biofilms. (A) *S. gordonii* DL1 were coincubated with 50 μM hydroxyaurones **HA2−6** or **G43**, and biofilm formation was measured at OD_{562} using the crystal violet protocol. (B) *S. sanguinis* SK36 were coincubated with 50 μM hydroxyaurones **HA2−6** or **G43**, and biofilm formation was measured at OD_{562} using the crystal violet protocol. Each experiment was repeated three times with triplicate microwells for each compound. Statistical significance was tested with one-way ANOVA. $p < 0.0001$.

was inhibited by 30−40% (Figure 5B). However, these effects were less pronounced than their effects on the *S. mutans* biofilm. For example, compounds **HA5** and **HA6** displayed about 95% inhibition of *S. mutans* biofilm at 50 μM (Figure 4C). These effects were also comparable to the control Gtf inhibitor **G43** reported from our laboratory previously. In addition, a side-by-side comparison of biofilm inhibitory effects of 25 μM **HA5** inhibited 80% of *S. mutans* biofilm, while it did not significantly reduce *S. sanguinis* biofilm and inhibited about 20% of *S. gordonii* biofilm (Figure 8G). Overall, this data suggests that hydroxyaurones have a high degree of selectivity toward inhibiting pathogenic biofilms compared to commensal biofilms.

Considering the potential of methoxyaurones and hydroxyaurones for further development, their biofilm inhibitory activities were further characterized in serial dilutions and IC_{50} values were determined. The hydroxyaurones were found to have lower IC_{50} values compared to the corresponding methoxyaurones (Table 1). Among methoxyaurones, 3,4-dimethoxyaurone **MA3** was found to be the most active analogue with an IC_{50} value of 49.40 μM. The 2,4,5-trimethoxyaurone **MA5** had a similar IC_{50} value of 52.81 μM and the 4-methoxyaurone **MA2** had an IC_{50} value of 107.80 μM, while 3,4-dimethoxy and 3,4,5-trimethoxyaurones were inactive. Interestingly, the unsubstituted aurone **MA1** was more potent than all methoxyaurones with an IC_{50} value of 33.61 μM. However, **MA1** also displayed about 80% inhibition of *S. mutans* growth at 50 μM, suggesting that its observed biofilm inhibition may be arising from its bactericidal activity.

Two hydroxyaurones 2,4,5-trihydroxyaurone (**HA5**) and 3,4,5-trihydroxyaurone (**HA6**) were found to be the most active derivatives with IC_{50} values of 6.42 and 18.92 μM, respectively. The 3,4-dihydroxyaurone **HA3** and 3,5-dihydroxyaurone **HA4** were found to be less active with IC_{50} values of 30.67 and 94.22 μM, respectively. Among these, **HA4** with no OH at the 4-position was less active than **HA3** with an OH group at the 4-position. Interestingly, the monohydroxy analogue **HA2** with an OH group at 4-position was found to be more active than the dihydroxyaurones **HA3** and **HA4**. It should be noted that both of our most active analogues **HA5** and **HA6** also contained an OH group at the 4-position, indicating the importance of the 4-OH group for the biofilm inhibitory activities of hydroxyaurones. This observation is further supported by our cocrystal structure of **HA5** in the GtfB active site, showing that the two oxygen atoms at the 4,5-position of the 2,4,5-trihydroxyphenyl moiety interacted with the key amino acid residues in the active site through coordination with a conserved Ca^{2+} ion (Figure 7). Of all of the aurone analogues synthesized, 2,4,5-trihydroxyaurone **HA5** (Figure 6E) was selected as our lead compound for further

https://doi.org/10.1021/acs.jmedchem.3c00272
J. Med. Chem. 2023, 66, 7909−7925

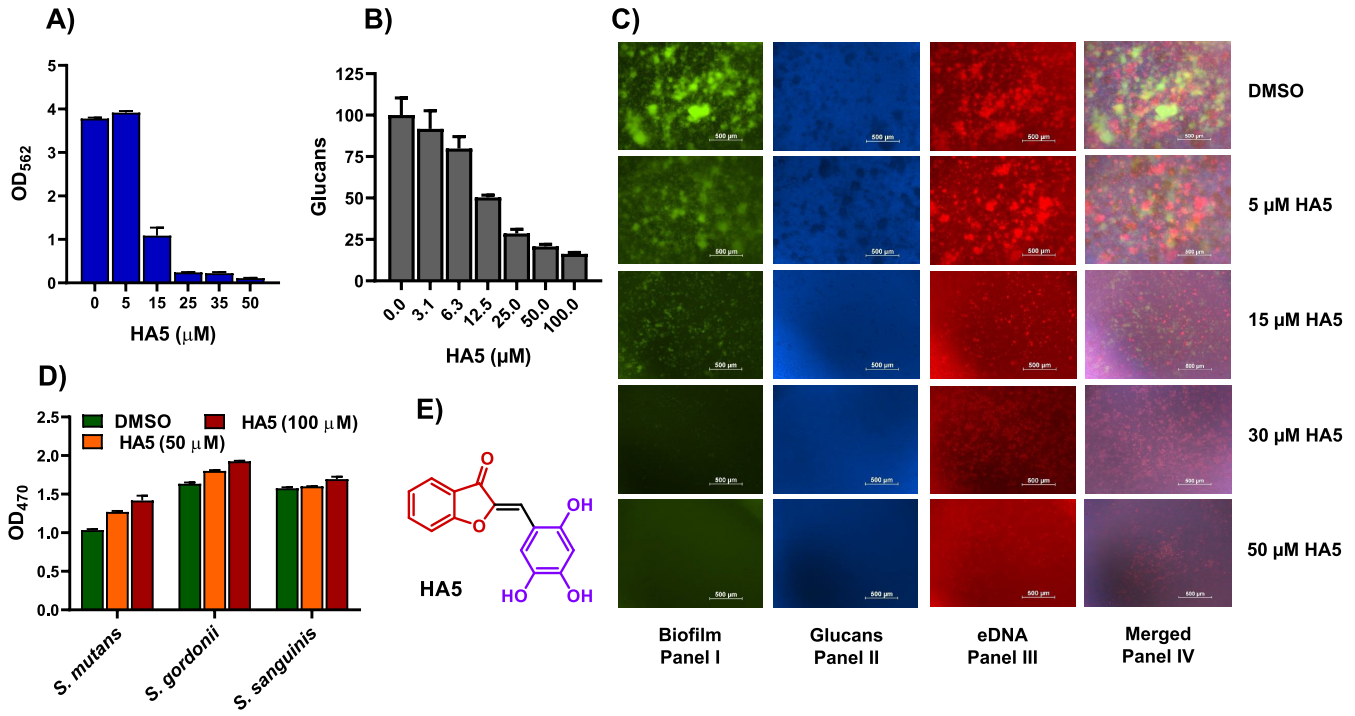

Figure 6. Biofilm inhibitory activities of compound **HA5**. (A) *S. mutans* UA159 were coincubated with **HA5** at various concentrations, and biofilm formation was measured at OD_{562} using the crystal violet protocol. (B) Gtfs precipitated from *S. mutans* culture were coincubated with **HA5** at various concentrations and the glucan production was quantified using cascade blue staining and subsequent image processing with ImageJ. (C) Representative fluorescence microscopy images of UA159 biofilms after 16 h of treatment with various concentrations of **HA5**. Bacterial cells were stained with Syto-9 (green, panel I); glucans were stained with Cascade Blue-dextran conjugated dye (blue, panel II); eDNA was stained with propidium iodide (red, panel III) and a merged image of all three staining images (panel IV). (D) *S. mutans* UA159, *S. gordonii* DL1, and *S. sanguinis* SK36 were coincubated with **HA5** at 50 and 100 μM and their growth was measured at OD_{470}. (E) Chemical structure of **HA5**. Each of the biofilm, glucan, and growth assays were conducted in triplicate and statistical significance was tested with one-way ANOVA. $p < 0.0001$.

analysis and encapsulation studies based on its potent biofilm inhibition, lack of growth inhibition, and improved solubility.

HA5 Inhibits *S. mutans* UA159 Biofilms, Glucan Production, and eDNA Levels. The anti-biofilm activities of **HA5** were further investigated by fluorescence microscopy imaging. Compound **HA5** displayed a dose-dependent inhibition of *S. mutans* biofilm as shown in Figure 6A. Staining of bacterial cells within biofilms with Syto-9 showed significant reduction in biofilms at 5 μM **HA5** and a complete inhibition at 50 μM **HA5** (Figure 6C, Panel I). The presence of glucans, which were stained with the Cascade Blue-dextran conjugated dye, was significantly reduced at 5 μM **HA5** and no glucan formation was evident at 50 μM **HA5** (Figure 6C, Panel II). In addition, propidium iodide was used to determine the presence of extracellular DNA (eDNA) in *S. mutans* biofilms. Again, there was a noticeable reduction of eDNA at 5 μM **HA5** and almost complete absence of eDNA at 50 μM **HA5** (Figure 6C, Panel III). These findings reaffirm that **HA5** inhibited *S. mutans* biofilms by preventing the synthesis of glucans and minimizing the presence of eDNA, two integral biofilm matrix elements crucial for *S. mutans* biofilm formation.

HA5 Inhibits Glucan Production of *S. mutans* UA159 in a Dose-Dependent Manner. The interspecies coadherence between *S. mutans* and other microorganisms in the oral cavity is critical for biofilm formation and cariogenicity. Although the mechanisms of such adhesions and coaggregations are not fully elucidated, it is believed that the extracellular polysaccharide (EPS) matrix of *S. mutans* has an important role in this process.[49,50] It is reported that glucans synthesized by Gtfs when incorporated into the tooth pellicle to provide enhanced binding sites for other microorganisms to form stable and persistent microcolonies, which provides mechanical stability to the EPS matrix.[50,51] Therefore, Gtf inhibition assays were performed to assess the ability of **HA5** to inhibit Gtfs and glucan production using a reported procedure and the IC_{50} value was calculated.[52] Compound **HA5** exhibited dose-dependent inhibition of glucan production by Gtfs with an IC_{50} value of 10.56 μM (Figure 6B). These findings reinforce the biofilm inhibitory activity of **HA5** and suggest that the compound inhibits biofilm formation by inhibiting the production of glucans by *S. mutans* Gtfs.

HA5 Does Not Affect the Growth of Commensal Streptococcal Species. To determine if compound **HA5** only selectively inhibits *S. mutans* biofilms over the growth of *S. mutans* and oral commensal species, the effects of **HA5** on the growth of two representative commensal oral streptococci, *S. gordonii* and *S. sanguinis*, along with *S. mutans* at 50 and 100 μM doses were evaluated. As shown in Figure 6D, compound **HA5** did not inhibit the growth of two commensals compared to the control group at these doses that are much higher than its biofilm IC_{50} value of 6.42 μM. Similarly, the compound did not inhibit *S. mutans* growth at these doses, suggesting that **HA5** selectively inhibited *S. mutans* biofilms without affecting its growth as well as the growth of commensal species *S. gordonii* and *S. sanguinis* (Figure 6D).

Structural Studies on HA5 in the Catalytic Domain of GtfB. Apo crystals of GtfB were obtained in the Index (Hampton Research) A3 crystallization condition using the hanging drop vapor diffusion technique producing reliably large enough (0.1−0.2 mm) tetragonal crystals for GtfB. Apo

https://doi.org/10.1021/acs.jmedchem.3c00272
J. Med. Chem. 2023, 66, 7909−7925

crystals of GtfB were soaked with **HA5** for 5−10 min (final concentration 1−2 mM; 20 mM stock solution of compound **HA5** in H_2O). The GtfB structure complexed with **HA5** diffracted to a resolution of 2.35 Å. Diffraction data for the inhibitor structure were collected at 100 K using the hybrid pixel DECTRIS Eiger 16 m detector at the SERCAT 22-ID beamline in the Advanced Photon Source (APS), Chicago. For cryoprotection of GtfB crystals, 20% ethylene glycol was added to the crystallization buffer. The collected data were processed using XDS[53] for initial indexing, merging, and scaling and were followed by optimization using Aimless[54] in CCP4.[55] The data collection statistics are shown in Table 2. The structure for GtfB was solved by molecular replacement using Phaser with a model for GtfB generated by the SWISS-MODEL web server based on the catalytic domain of GtfC (3AIE). Refinement was performed using a combination of Refmac5[56] in CCP4[55] and Phenix.[57] MOGUL (CSD release) restraints for compound **HA5** were based on the CCDC small-molecule database and obtained from the Grade web server. Compound **HA5** is unknown to PDB, and therefore, was sketched in ChemAxon and the resulting SMILES notation provided the initial input. Coot was used for all model building[58] and figures were created with PyMOL (version 2.5.0, Schrödinger, LLC). Validation of the model quality was performed using Phenix and the wwPDB validation service. The ligand was validated using the same set of MOGUL restraints described above. The conserved Ca^{2+} site in the structure of GtfB was verified with the CheckMyMetal web server. The protein structure has been deposited in PDB (PDB ID: 8FG8). Final refinement statistics are presented in Table 2.

Table 2. Data Collection and Refinement Statistics for GtfB in Complex with HA5

data collection	
space group	$P4_322$
unit cell parameters [Å]	$a = b = 150.46$, $c = 304.95$
resolution [Å]	87.25−2.35 (2.39−2.35)
unique reflections	142,674 (7062)
completeness [%]	98.5 (99.2)
multiplicity	7.4 (7.2)
R_{merge} [%]	19.1 (210.7)
R_{pim} [%]	6.5 (71.2)
$CC_{1/2}$ (2.39−2.35 Å)	0.350
CC* (2.39−2.35 Å)	0.720
$I/\sigma(I)$	8.1 (1.1)
refinement	
resolution [Å]	73.04−2.35 (2.41−2.35)
no. of reflections	139,861 (10356)
completeness [%]	96.1 (97.6)
R_{work} [%]	20.5 (33.6)
R_{free} [%]	23.3 (35.5)
Wilson B [Å^2]	48.0
average B-factors [Å^2]	
overall	57.9 (13,785 atoms)
protein, Ca^{2+}, HA_5, BTB	57.8 (13,091 atoms), 55.9 (3 ions), 83.7 (40 atoms), 73.9 (28 atoms)
SO_4^{2-}, waters	97.7 (125 atoms), 47.2 (503 atoms)
R_{msd} bonds [Å]	0.013
R_{msd} angles [deg]	1.74
CC ($F_o - F_c$)	0.95
Ramachandran [%]	95.9 favored (outliers 0.7)
clash score	3.76
molprobity score	1.44

Interactions of HA5 within the GtfB Active Site. To define the underlying mechanism of **HA5**'s ability to inhibit Gtfs and biofilm, a high-resolution cocrystal structure of **HA5** with the catalytic domain of GtfB was resolved. The analysis of the **GtfB/HA5** cocrystal structure revealed that the inhibitor **HA5** was crystallized along with Bis−Tris (BTB), a chemical component of the buffer used in the crystallization studies (Figure 7A−B). Inhibitor **HA5** was found to adopt a classic $\pi-\pi$ stacking interaction with the Trp491 residue in the GtfB active site (Figure 7C). In the structure, only water-mediated hydrogen bonds are observed for **HA5**, which differs from the reported *in silico* docking results with the inhibitor **G43**, which highlighted hydrogen bond interactions of **G43** with the three active site residues Asp451, Glu489, and Asp562.[19] In the crystal structure of **HA5**, the inhibitor makes only hydrophobic contact with these residues (Figure 7C). For the sucrose to undergo invertase activity, the glucose molecule will nest within the −1 subsite, which consists of residues Arg449, Asp451, Glu489, His561, Asp562, and Tyr890. And the fructose interacts with the +1 subsite that consists of Tyr404, Leu407, and Trp491. These nomenclatures are adopted for sugar binding sites for glycosylhydrolases.[59] The inhibitor **HA5** in this crystal structure binds to subsites +1 and +2 that include the residues Asn511, Arg514, and Asp567. Inhibitor **HA5** makes hydrophobic interactions with a total of 15 interface residues in these two subsites. 50% of its solvent-accessible surface area is buried in the protein−ligand interactions. In chain B of GtfB, two oxygen atoms at the 4,5-position of the 2,4,5-trihydroxyphenyl moiety of the inhibitor **HA5** coordinated with a conserved Ca^{2+} ion and extend their interaction with Asp451 and Glu489 (Figure 7C). The 4-OH group on the benzene ring of **HA5** interacts with Tyr404. In chain A of GtfB, the 2,4,5-trihydroxyphenyl moiety is rotated around the methylidene atom with respect to the benzofuran ring system, allowing a hydrogen bond with a BTB buffer molecule (buffer of the crystallization condition) within the active site. The result of finding BTB in the GtfB active site is not surprising since Tris as an ethanolamine derivative has been previously reported as a competitive inhibitor of GtfB.[60] Binding of the BTB in this structure occurs in −1 subsite and overlaps with the proposed binding of the glucosyl moiety of sucrose. The BTB molecule provides 11 hydrogen bonds to protein residues within the active site. Placements of **HA5** and BTB in both subunits were not only verified in $2mF_o - DF_c$ maps at 1σ contour level but also in Polder difference omit maps at 5 sigma contour levels (Figure S1).

We realize that HA5 is a polyhydroxy compound that contains a Michael acceptor functionality, which raises concerns about nonspecific and covalent binding. However, it is unlikely that HA5 is influenced by these mechanisms because our HA5/GtfB cocrystal structure clearly shows its binding in the catalytic site of GtfB with specific interactions with the Ca^{2+} ion and with active site residues and it does not show any covalent bond to its Michael acceptor site. To further validate that HA5 is not a Michael acceptor, the Gtf inhibition IC_{50} values for HA5 in the presence and absence of a nucleophilic reagent β-mercaptoethanol (BME, 1 mM) have been determined and shown that BME does not reduce the Gtf inhibitory activity (7.84 vs 10.56 μM).[61] In addition, the Gtf

https://doi.org/10.1021/acs.jmedchem.3c00272
J. Med. Chem. 2023, 66, 7909−7925

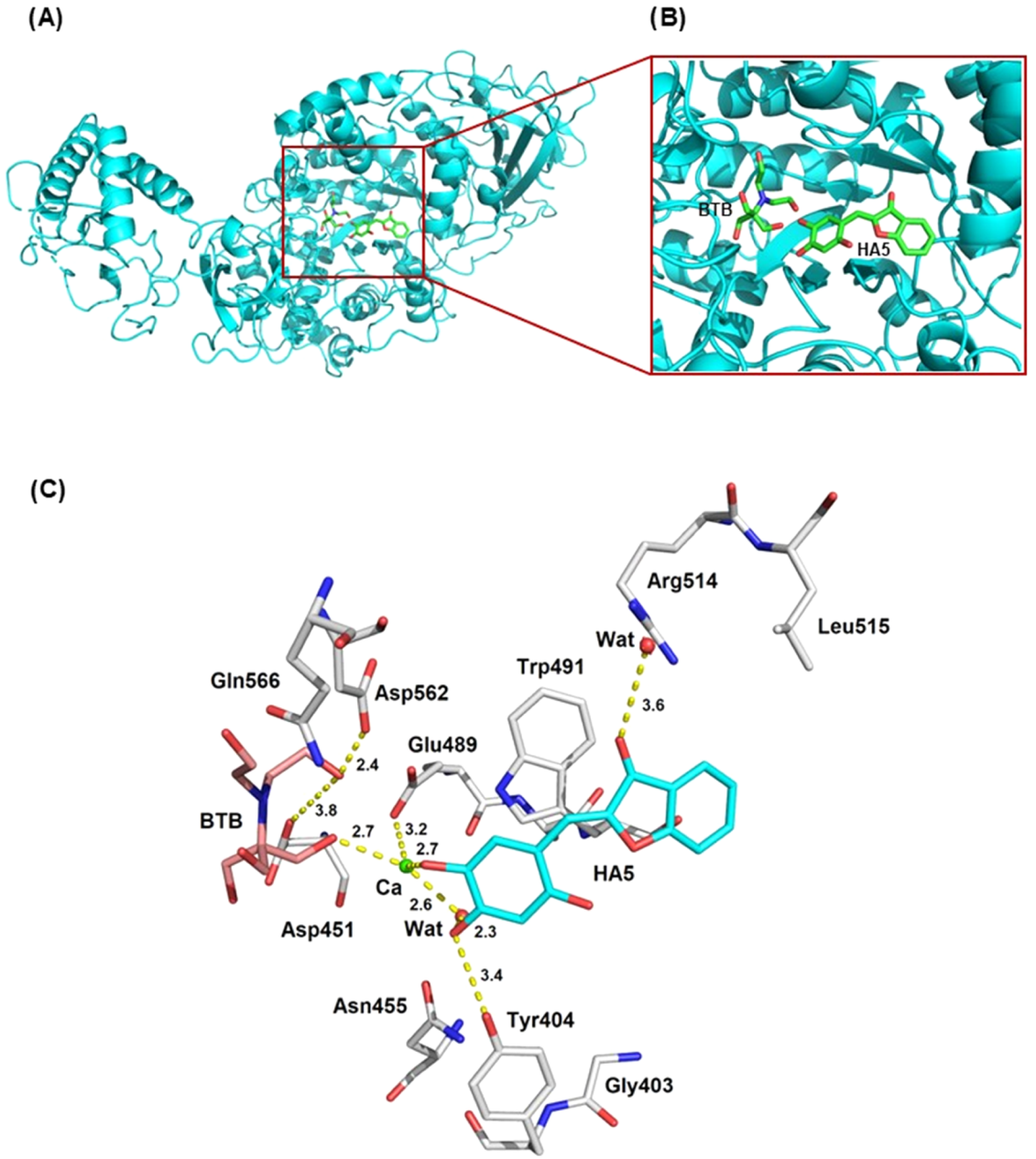

Figure 7. (A) High-resolution X-ray cocrystal structure (PDB ID: 8FG8) of the inhibitor **HA5** with the catalytic domain of GtfB. Inhibitor **HA5** and BTB are displayed as green sticks. (B) Expansion of the GtfB binding site showing the binding mode of **HA5**. (C) Key active site interactions of **HA5** with active site residues (gray sticks) along with its H-bong interactions with water (Wat) molecules and calcium (Ca^{2+}) ion depicted as yellow dotted lines. Inhibitor **HA5** is depicted as light blue sticks and BTB is depicted as lavender sticks.

inhibition IC_{50} values for HA5 in the presence and absence of a detergent Triton-X-100 have been determined to show that it is not a nonspecific inhibitor.[62] Triton-X-100 did not reduce the Gtf inhibitory activity (5.16 vs 10.56 μM) of HA5, suggesting that the observed Gtf inhibition is not due to nonspecific binding.

Hydrogel-Encapsulated Biofilm Inhibitors (HEBI). Hydrophilicity, the ease of chemical modification and structural stability of hydrogel matrices ensures excellent biocompatibility and versatility for its use in biomedical applications. Poly(methacrylic acid) (PMAA) multilayer hydrogel is an excellent platform for the pH-triggered drug delivery of the biofilm inhibitors as these respond to varying pH due to the existence of ionizable pendant groups (*e.g.*, $-COOH$ and $-NH_2$) in the network. In our previous studies, PMAA hydrogels have been prepared by layer-by-layer (LbL) assembly of hydrogen-bonded polymers of PMAA and poly(*N*-vinylpyrrolidone) (PVPON). The PMAA and PVPON layers were alternately adsorbed onto surfaces of porous inorganic microparticles of manganese oxide, followed by chemical cross-linking of PMAA with ethylenediamine and dissolution of the manganese oxide template microparticles.[63−65] The nanoscale multilayers of chemically cross-linked PMAA result in the interconnected porous hydrogel structure, which provides excellent drug loading capacity. In addition, the pH responsiveness of the hydrogel can be easily tuned during particle formation by using pH-sensitive cross-linkers.[66] We have recently demonstrated the biocompatibility and degrad-

https://doi.org/10.1021/acs.jmedchem.3c00272
J. Med. Chem. 2023, 66, 7909−7925

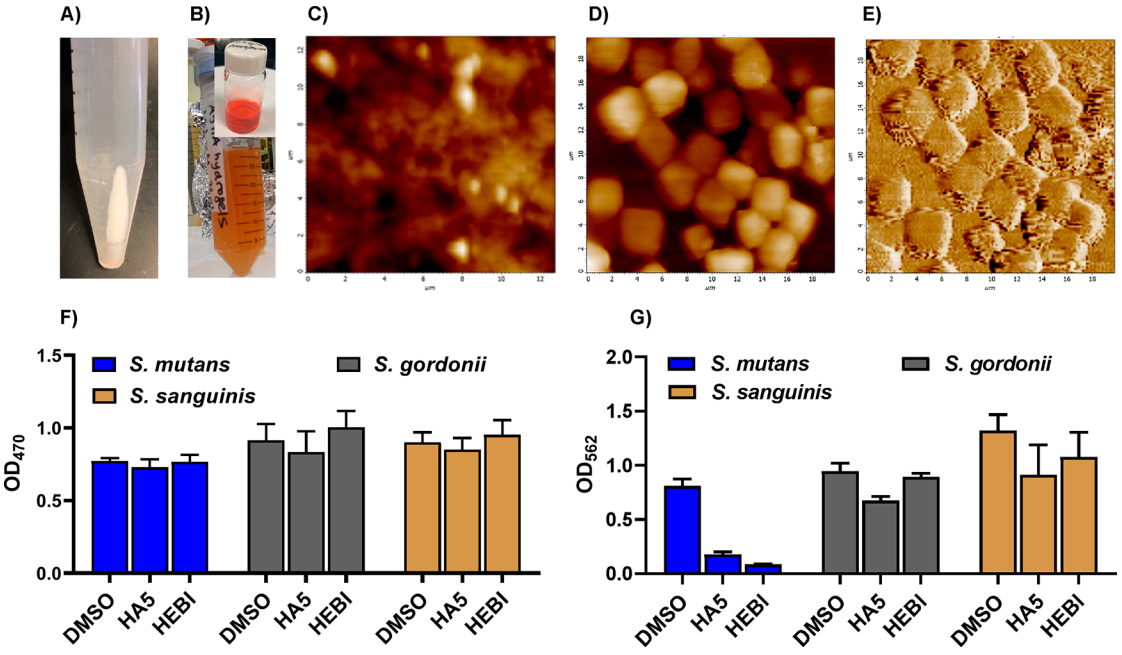

Figure 8. (A) Optical images of empty $(PMAA)_5$ hydrogel microparticles. (B) **HA5**-loaded hydrogel **HEBI** and **HA5** in methanol (insert B). (C) Atomic force microscopy (AFM) topography images of a tooth surface with a height scale of 280 nm. (D) AFM height image after $(PMAA)_5$ hydrogel adsorption; cubical hydrogel particles are clearly seen sticking to the tooth surface. (E) AFM Amplitude error image of empty $(PMAA)_5$ hydrogels dried on the surface of a tooth. Scan size is 20 μm^2 in both images, the height (z)-scale is 1.7 μm. (F) *S. mutans* UA159 and two bacterial commensal species *S. gordonii* DL1 or *S. sanguinis* SK36 were coincubated with **HA5** or **HEBI** at 25 μM and their growth was measured at OD_{470}. (G) *S. mutans* UA159, *S. gordonii* DL1, or *S. sanguinis* SK36 were coincubated with 25 μM **HA5** or **HEBI** and biofilm formation was measured at OD_{562} using the crystal violet protocol. Each of the biofilm and growth assays were conducted in triplicate and statistical significance was tested with one-way ANOVA. $p < 0.0001$.

ability of hydrogel biomaterial in the delivery of small-molecule drugs.[65]

Encapsulation of HA5 Inside $(PMAA)_5$ Hydrogel Microparticles. Compound **HA5** was encapsulated in the $(PMAA)_5$ hydrogel cubes through post-loading by soaking the hydrogels in 5 mg/mL solution of **HA5** in methanol for 48 h in the dark (Figure 8A,B). The free, nonencapsulated **HA5** was removed from particle solution by rinsing with HEPES buffer (pH = 7.4) five times using centrifugation at 5000 rpm for 10 min. The **HA5** quantification was carried out with UV−visible spectroscopy (NanoDrop One C, ThermoFisher) at λ = 448 nm using an **HA5** calibration curve. The drug solution was analyzed before and after the exposure to the hydrogel particles and the differences in the absorbance spectra were used to determine the loading of the drug into the hydrogel network. The loading capacity was found to be 5.5×10^{-3} ng of **HA5** per particle. To demonstrate the tooth adhesion of $(PMAA)_5$ hydrogel microparticles, a drop of the hydrogel particle dispersion was placed on the tooth surface and dried at room temperature for 10 min in a Petri dish and the morphology of the hydrogels was analyzed using atomic force microscopy (AFM NTEGRA II microscope: NT-MDT) imaging. Freshly extracted, intact third molars with flat surfaces obtained from Dr. Nathaniel Lawson's lab (UAB School of Dentistry, IRB-300001291) were used in these studies. The AFM silicon probes NSG30 (NT-MDT; resonance frequency, 240−440 kHz; force constant, 22−100 N m^{-1}; tip radii, 10 nm; scan rate, 0.5 Hz) were used for imaging the tooth surfaces in tapping mode before and after hydrogel adhesion. The AFM height image shows that the bare tooth surface displays natural topography (Figure 8C) with a height scale of 280 nm. After hydrogel addition, the cubical hydrogel particles are seen to adhere to the tooth surface (Figure 8D−E). The height of the dried hydrogel cubes was determined using cross-section profiles, which indicated an average particle height of 1.3 ± 0.2 μm. The hydrogel cubes decreased in size compared to their size in solution due to the hydrogel shrinkage upon drying.[65]

Inhibition of Biofilms and Planktonic Growth by HEBI. Effects of **HEBI** and **HA5** on biofilms and planktonic growth of *S. mutans* and two commensal streptococci *S. gordonii* and *S. sanguinis* were evaluated at a single treatment dose of 25 μM. **HEBI** inhibited about 85−90% of *S. mutans* biofilms, which is comparable to 90% inhibition by **HA5** (Figure 8G). **HEBI** did not significantly inhibit the biofilms of commensal species *S. gordonii* and *S. sanguinis* at this concentration. As expected, based on our previous data, **HEBI** or **HA5** did not affect the planktonic growth of *S. mutans* or the commensal species *S. gordonii* and *S. sanguinis* at the treatment concentration of 25 μM (Figure 8F).

Reduction of *S. mutans* Virulence *In Vivo* by HA5 or HEBI. The effects of compounds **HA5** and **HEBI** on *S. mutans* virulence were evaluated using a well-established gnotobiotic rat model of dental caries.[67] Hydrogel microparticles with no drug were used to ensure that the observed antivirulence activity with **HEBI** was not related to the hydrogel material. The standard NaF (250 ppm) was included as a positive control. A (vehicle + infection only) group was included as a negative control. All rats in the experimental groups and control groups were colonized with *S. mutans* UA159. A 4-week treatment of *S. mutans* UA159-infected gnotobiotic rats with 100 μM **HA5** or **HEBI** resulted in significant reduction in buccal and sulcal caries scores compared to control groups. Similar reductions in caries scores were also observed in proximal enamel caries scores (Table 3). We were unable to

https://doi.org/10.1021/acs.jmedchem.3c00272
J. Med. Chem. 2023, 66, 7909−7925

Table 3. Effect of HEBI or HA5 Treatment on *S. mutans* UA159-Induced Dental Caries[a]

treatment group	buccal mean caries scores (±SEM)				sulcal mean caries scores (±SEM)				proximal mean caries scores (±SEM)
	E	Ds	Dm	Dx	E	Ds	Dm	Dx	E
UA159 untreated	14.6 ± 0.2	10.2 ± 0.4	6.0 ± 0.0	3.2 ± 0.5	25.6 ± 0.2	17.8 ± 0.2	10.4 ± 0.2	4.2 ± 0.2	6.0 ± 0.0
hydrogel (no drug)	15.0 ± 0.3	9.6 ± 0.8	6.4 ± 0.7	3.8 ± 1.1	27.0 ± 0.5	19.6 ± 0.4	12.4 ± 0.9	6.0 ± 0.5	6.8 ± 0.5
HEBI (100 μM)	7.4 ± 1.1	5.2 ± 1.2	2.4 ± 0.7	1.4 ± 0.6	16.0 ± 0.6	12.6 ± 0.2	6.8 ± 0.7	4.0 ± 0.0	3.6 ± 0.4
HA5 (100 μM)	11.0 ± 0.3	6.0 ± 0.4	3.8 ± 0.2	2.0 ± 0.7	22.0 ± 0.6	16.2 ± 0.4	8.8 ± 0.9	4.4 ± 0.9	4.0 ± 0.0
NaF (250 ppm)	5.0 ± 0.7	2.4 ± 0.8	1.0 ± 0.8	0.0 ± 0.0	14.2 ± 0.7	11.2 ± 0.4	4.6 ± 0.2	1.0 ± 0.3	1.2 ± 0.8

[a]Enamel (E); dentinal slight (Ds); dentinal moderate (Dm); and dentinal extensive (Dx); proximal dentinal scores are not included as there were no significant proximal dentinal lesions for the control and treated groups in this study.

evaluate the effect of the treatment on proximal dentinal scores as there were no significant proximal dentinal lesions for the control and treated groups in this study. In comparison, the group treated with hydrogel (no drug) did not show any inhibition compared to the control group, suggesting that the hydrogel as such has no antivirulence activity (Table 3). The observed reduction in caries scores by **HA5** and **HEBI** was similar with **HEBI** displaying slightly better *in vivo* activity, possibly due to the pH-dependent slow release. The observed reduction in caries scores by **HA5** or **HEBI** was lower than the 250 ppm NaF treatment. However, it should be noted that the concentration of NaF (250 ppm = 5.95 mM) is about 59-fold higher than **HA5** (100 μM). At the end of the study, the animals were euthanized and their mandibles excised for microbiological analysis of plaque samples on MS agar plates and BAP and for scoring of caries by the method of Keyes[68] to determine the bacterial colonization. The effect on bacterial colonization was not significant in **HA5**- or **HEBI**-treated animals when compared to the control group, while the bacterial colonization appears to be slightly reduced in unloaded hydrogel-treated rats. This data suggests that **HA5** and **HEBI** are less toxic to bacteria (Table 4). Moreover, the

Table 4. Effect of HEBI or HA5 Treatment on *S. mutans* UA159 CFU and the Body Weight of the Animals[a]

treatment group	CFU/mL ($\times 10^6$)		animals	
	MS	BAP	weight (g)	number
UA159 untreated	4.2 ± 1.4	5.6 ± 1.6	141 ± 13	5
hydrogel (no drug)	1.6 ± 0.5	2.4 ± 0.7	130 ± 9	5
HEBI (100 μM)	5.2 ± 1.4	5.5 ± 1.4	145 ± 12	5
HA5 (100 μM)	2.5 ± 0.8	3.0 ± 1.0	137 ± 13	5
NaF (250 ppm)	3.4 ± 0.5	4.0 ± 0.9	161 ± 13	5

[a]Colony-forming unit (CFU); mitis salivarius (MS); blood agar plates (BAP).

rats treated with the compound **HA5** or **HEBI** did not experience any weight loss over the course of the study in comparison with the control group, suggesting that they are nontoxic (Table 4). Overall, our data suggest that **HEBI** can release **HA5** in the rat's oral cavity under the acidic conditions of dental caries, and the reduction in caries scores produced by **HEBI** is comparable to that observed for **HA5** treatment alone. These results also indicate that the compound **HA5** or **HEBI** selectively targets *S. mutans* virulence factors; Gtfs and Gtf-mediated biofilm formation, rather than a simple inhibition of bacterial growth, are very effective in inhibiting dental caries *in vivo*. All *in vivo* experimental protocols were approved by the University of Alabama at Birmingham Institutional Animal Care and Use Committee (Protocol No. IACUC-20047). The methods were carried out in accordance with the relevant guidelines and regulations.

CONCLUSIONS

In conclusion, we have developed novel small-molecule inhibitors of *S. mutans* glucosyl transferases as selective biofilm inhibitors that do not affect the growth of oral commensal bacteria. The solubility and biofilm inhibitory activities of the lead compound were optimized for drug encapsulation. The optimized lead compound **HA5** inhibited *S. mutans* biofilm with an IC_{50} value of 6.42 μM without affecting its growth. Compound **HA5** was further evaluated for its effect on the growth of oral commensal bacterial species *S. gordonii* and *S. sanguinis* and showed that it does not inhibit the growth of *S. gordonii* and *S. sanguinis* at 100 μM, which is 14-fold higher dose than its biofilm IC_{50} value. The binding of **HA5** to the glucosyl transferase GtfB has been demonstrated by resolving a high-resolution X-ray cocrystal structure of **HA5** with the catalytic domain of GtfB and mapped its active site interactions. Compound **HA5** inhibited *S. mutans* Gtfs and glucan production with an IC_{50} value of 10.56 μM in a Gtf inhibition assay. Compound **HA5** was encapsulated into pH-responsive hydrogel microparticles to generate a hydrogel-encapsulated biofilm inhibitor (**HEBI**), which displayed selective inhibition of the *S. mutans* biofilm similar to **HA5**. The effects of **HA5** or **HEBI** on the biofilm on commensal species *S. gordonii* and *S. sanguinis* were minimal at 25 μM. A 4-week treatment of *S. mutans* UA159-infected gnotobiotic rats with 100 μM **HA5** or **HEBI** resulted in significant reduction in buccal, sulcal, and proximal dental caries scores compared to control groups, demonstrating their antivirulence activities *in vivo* without affecting the bacterial colonization significantly. The rats treated with **HA5** or **HEBI** did not experience any weight loss over the course of the study in comparison with the control group, suggesting that the compound and material are nontoxic. Overall, our *in vivo* data suggests that **HEBI** can release **HA5** in the rat oral cavity under the acidic conditions of dental caries infection and reduce dental caries, and the results are comparable to those observed for **HA5** treatment alone. Overall, the results of this study suggest that compound **HA5** or **HEBI** selectively targeted *S. mutans* Gtfs and Gtf-mediated biofilm formation, rather than a simple inhibition of

https://doi.org/10.1021/acs.jmedchem.3c00272
J. Med. Chem. 2023, 66, 7909−7925

bacterial growth, demonstrating the potential of this compound and material to be developed further as novel dental caries treatments.

EXPERIMENTAL SECTION

General Considerations. ^{1}H NMR and ^{13}C NMR spectra were recorded on Bruker Avance Neo 400 and Avance II 700 spectrometers using TMS or appropriate solvent signals as internal standard. The chemical shift values are given in parts per million (ppm) relative to the internal standard used and the coupling constants (J) are given in hertz (Hz). High-resolution mass spectra (HRMS) were recorded using a Waters AutoSpec-Ultima NT magnetic sector mass spectrometer with an Electron Impact (EI) Ionization source. The mass analyzer is an electric−magnetic−electric (EBE) sector (a double focusing sector). Anhydrous solvents used for reactions were purchased in Sure-Seal bottles from Aldrich Chemical Company. Other chemical reagents were purchased from Aldrich or Fisher Chemical Companies and used as received. Reactions were monitored with thin layer chromatography (TLC), which was done on silica gel plates with a fluorescent indicator (Silicycle, silica gel, UV254, 25 μm plates). The TLC spots were observed under UV light with wavelengths 254 and 365 nm. The reaction mixtures were purified by column chromatography using Si gel (32−63 μm) from Dynamic Adsorbent, Inc. Melting points were determined on a Mel-Temp II melting point apparatus and are uncorrected. All tested compounds have ≥95% purity as determined by high-performance liquid chromatography (HPLC). HPLC traces were obtained using Shimadzu SPD-M20A. Solubility of compounds was determined by the UV-spectroscopy method using an Agilent Cary 60 UV−vis spectrophotometer. HPLC analysis of compounds was conducted using Kinetex 5 μm C18 100 Å, LC Column 150 mm × 4.6 mm (Phenomenex), compound = 3 mM, 5 μL injection. Mobile phase A (0.1% TFA in H_2O) and mobile phase B (0.1% TFA in acetonitrile) were used as a binary gradient. Binary gradient: 0−3 min (10−95% mobile phase B), 3−5 min (95% mobile phase B); 5−5.1 min (95−10% mobile phase B); 5.1−6 min (10% mobile phase B). Flow rate: 1.0 mL/min. Oven temperature: 30 °C. Signals were analyzed using a 254 nm UV detector. A chromatogram of the mobile phase buffer (20 μL) was obtained for comparison.

Poly(ethyleneimine) (PEI, average M_w 25,000), ethylenediamine (EDA), manganese sulfate monohydrate, ammonium bicarbonate, and 1-ethyl-3-(3-(dimethylamino)propyl)-carbodiimide hydrochloride were purchased from Sigma-Aldrich. Poly(methacrylic acid) (PMAA, average M_w 22,000 g mol^{-1}, $Đ$ = 1.3) was purchased from Fisher Scientific. Ultrapure deionized (DI) water with a resistivity of 18.2 MΩ·cm at 25 °C was used in all experiments. Monobasic and dibasic sodium phosphate (Fisher Scientific) were used for the preparation of polymer and buffer solutions. Poly(*N*-vinylpyrrolidone) (PVPON, M_w 10,000 g mol^{-1}) was from Sigma-Aldrich. Slices of human teeth were provided by Dr. Nathaniel Lawson (UAB School of Dentistry, IRB-300001291) and used as received.

The bacterial strains, *S. mutans* UA159, *S. gordonii* DL1, and *S. sanguinis* SK36 were inoculated statically at 37 °C under 5% CO_2 in Todd Hewitt Broth (THB) for 24 h. The cultures were then diluted with fresh THB (1:5) and reinoculated until optical density at 470 nm (OD_{470}) reached 1. The optical density was read using a BioTek 800TS microplate reader at 470 nm for bacterial growth and 562 nm for biofilms stained with crystal violet. Data was plotted in Graphpad Prism9.

General Procedure for the Synthesis of Chalcones (3a−f). To a solution of 2-hydroxyacetophenone **1** (1 mmol) and benzaldehyde **2a** (1 mmol) in EtOH (10 mL), an aqueous solution of KOH (40%, 1 mL) was added, and the reaction mixture was stirred at room temperature for 12 h. TLC examination (30% EtOAc in hexanes) indicated the completion of the reaction. The reaction mixture was then poured over crushed ice and acidified the pH to 2 using 1.0 N HCl. The precipitate formed was filtered, washed with copious amounts of water, and dried to obtain the crude product, which was purified on column chromatography over Si gel using 10% EtOAc in hexanes as the eluent to afford clean chalcones **3a−f**. All chalcone products were characterized by ^{1}H NMR, ^{13}C NMR, and HRMS as follows.

*1-(2-Hydroxyphenyl)-3-phenyl-2-propen-1-one (**3a**).* 61.9% yield, yellow solid; mp 89−90 °C; ^{1}H NMR (700 MHz, $CDCl_3$) δ: 12.84 (s, 1H), 7.94−7.92 (m, 2H), 7.68−7.66 (m, 3H), 7.52−7.49 (m, 1H), 7.45 (t, 3H, J = 3.1 Hz), 7.04 (d, 1H, J = 8.5 Hz), 6.95 (t, 1H, J = 7.6 Hz); ^{13}C NMR (700 MHz, $CDCl_3$) δ: 193.7, 163.6, 145.5, 136.4, 134.6, 130.9, 129.7, 129.0, 128.7, 120.1, 120.0, 118.9, 118.6; HRMS $[M - H]^-$ calcd for $C_{15}H_{12}O_2$ 223.0759, found 223.0763.

*1-(2-Hydroxyphenyl)-3-(4′-methoxyphenyl)-2-propen-1-one (**3b**).* 36.5% yield, yellow solid; mp 93−95 °C; ^{1}H NMR (700 MHz, $CDCl_3$) δ: 12.96 (s, 1H), 7.93−7.89 (m, 2H), 7.63 (d, 2H, J = 8.6 Hz), 7.54 (d, 1H, J = 15.4 Hz), 7.49 (t, 1H, J = 7.7 Hz), 7.02 (d, 1H, J = 8.3 Hz), 6.96−6.93 (m, 3H), 3.86 (s, 3H); ^{13}C NMR (700 MHz, $CDCl_3$) δ: 193.7, 163.6, 162.0, 145.4, 136.2, 130.6, 129.5, 127.3, 120.1, 118.8, 118.6, 117.6, 114.5, 55.5; HRMS $[M + H]^+$ calcd for $C_{16}H_{14}O_3$ 255.1021, found 255.1014.

*3-(3′,4′-Dimethoxyphenyl)-1-(2-hydroxyphenyl)prop-2-en-1-one (**3c**).* 53.0% yield, yellow solid; mp 115−117 °C; ^{1}H NMR (400 MHz, $CDCl_3$) δ: 12.94 (s, 1H), 7.94 (dd, 1H, J = 8.1, 1.6 Hz), 7.89 (d, 1H, J = 15.4 Hz), 7.53 (d, 1H, J = 15.4 Hz), 7.52−7.47 (m, 1H), 7.29−7.26 (m, 1H), 7.18 (d, 1H), 7.03 (dd, 1H, J = 8.3 Hz), 6.97−6.91 (m, 2H), 3.97 (s, 3H), 3.95 (s, 3H); ^{13}C NMR (700 MHz, $CDCl_3$) δ: 193.6, 163.6, 151.9, 149.4, 145.8, 136.3, 129.6, 127.7, 123.7, 120.2, 118.8, 118.7, 117.8, 111.2, 110.3, 56.1 (2); HRMS $[M - H]^+$ calcd for $C_{17}H_{16}O_4$ 283.0970, found 283.0969.

*3-(3′,5′-Dimethoxyphenyl)-1-(2-hydroxyphenyl)prop-2-en-1-one (**3d**).* 78.0% yield, yellow solid; mp 107−109 °C; ^{1}H NMR (700 MHz, $CDCl_3$) δ: 12.80 (s, 1H), 7.90 (d, 1H, J = 7.7 Hz), 7.81 (d, 1H, J = 15.4 Hz), 7.58 (d, 1H, J = 15.4 Hz), 7.49 (t, 1H, J = 8.4 Hz), 7.02 (d, 1H, J = 8.4 Hz), 6.93 (t, 1H, J = 7.7 Hz), 6.77 (d, 2H, J = 1.4 Hz), 6.56 (t, 1H, J = 1.4 Hz), 3.83 (s, 6H); ^{13}C NMR (700 MHz, $CDCl_3$) δ: 193.6, 163.5, 161.0, 145.4, 136.4, 136.4, 129.6, 120.5, 119.9, 118.8, 118.6, 106.5, 103.0, 55.4; HRMS $[M - H]^+$ calcd for $C_{17}H_{16}O_4$ 283.0970, found 283.0969.

*1-(2-Hydroxyphenyl)-3-(2′,4′,5′-trimethoxyphenyl)prop-2-en-1-one (**3e**).* 90.0% yield, orange solid; mp 135−137 °C; ^{1}H NMR (700 MHz, $CDCl_3$) δ: 13.08 (s, 1H), 8.21 (d, 1H, J = 15.4 Hz), 7.91 (dd, 1H, J = 7.7, 7.0 Hz), 7.60 (d, 1H, J = 15.4 Hz), 7.46 (dd, 1H, J = 8.4, 7.0 Hz), 6.99 (d, 1H, J = 8.3 Hz), 6.92 (t, 1H, J = 7.9 Hz), 6.5 (s, 1H), 3.94 (s, 3H), 3.92 (s, 3H), 3.90 (s, 3H); ^{13}C NMR (700 MHz, $CDCl_3$) δ: 194.0, 163.5, 155.1, 152.9, 143.2, 140.9, 135.8, 129.5, 120.2, 118.6, 118.4, 117.7, 115.1, 111.7, 96.6, 56.5, 56.2, 56.0; HRMS calcd for $C_{18}H_{18}O_5$ 314.1154, found 314.1151.

*1-(2-Hydroxyphenyl)-3-(3′,4′,5′-trimethoxyphenyl)prop-2-en-1-one (**3f**).* 85.4% yield, yellow solid; mp 155−157 °C; ^{1}H NMR (700 MHz, $CDCl_3$) δ: 12.86 (s, 1H), 7.92 (d, 1H, J = 7.9 Hz), 7.83 (d, 1H, J = 15.3 Hz), 7.53 (d, 1H, J = 15.3 Hz), 7.49 (t, 1H, J = 7.7 Hz), 7.02 (d, 1H, J = 8.2 Hz), 6.94 (t, 1H, J = 7.5 Hz), 6.87 (s, 2H), 3.93 (s, 6H), 3.91 (s, 3H); ^{13}C NMR (700 MHz, $CDCl_3$) δ: 193.5, 163.6, 153.5, 145.6, 140.8, 136.4, 130.0, 129.6, 120.0, 119.2, 118.8, 118.6, 105.9, 61.0, 56.2; HRMS $[M - H]^+$ calcd for $C_{18}H_{18}O_5$ 313.1076, found 313.1082.

General Procedure for the Synthesis of Methoxyaurones (MA1−6). Chalcones **3a−f** (0.6 mmol) were added to a homogeneous solution of $Hg(OAc)_2$ (0.221 g, 0.7 mmol) in anhydrous pyridine (20 mL) and the reaction mixture was heated at 110 °C for 12 h. The completion of reaction was marked by consumption of starting material and formation of a single product as visualized by TLC (50% EtOAc in hexanes). The reaction mixture was then quenched with ice and acidified to pH 2 by adding 1.0 N HCl. It was extracted in EtOAc (4 × 50 mL), and the combined extract was washed with water (2 × 50 mL), brine (1 × 50 mL), and dried over anhydrous Na_2SO_4. The drying agent was filtered off and the filtrate was concentrated *in vacuo* to obtain pure solid products **MA1−6**. All products were characterized by ^{1}H NMR, ^{13}C NMR, and HRMS as follows.

*2-(Phenylmethylidene)-2,3-dihydro-1-benzofuran-3-one (**MA1**).* 78.8% yield, off-white or beige solid; mp 110−111 °C; ^{1}H NMR

https://doi.org/10.1021/acs.jmedchem.3c00272
J. Med. Chem. 2023, 66, 7909−7925

(400 MHz, $CDCl_3$) δ: 7.92 (d, 2H, J = 7.5 Hz), 7.81 (d, 1H, J = 8.4 Hz), 7.66−7.64 (m, 1H), 7.46 (t, 2H, J = 7.8 Hz), 7.42−7.40 (m, 1H), 7.34 (d, 1H, J = 8.4 Hz), 7.22 (t, 1H, J = 7.4 Hz), 6.90 (s, 1H); ^{13}C NMR (700 MHz, $CDCl_3$) δ: 184.8, 166.2, 146.9, 136.9, 132.3, 131.6, 129.9, 128.9, 124.7, 123.5, 121.6, 113.1, 113.0; HRMS $[M - H]^+$ calcd for $C_{15}H_{10}O_2$ 221.0603, found 221.0596.

*2-[(4′-Methoxyphenyl)methylidene]-2,3-dihydro-1-benzofuran-3-one (**MA2**).* 92.5% yield, yellow solid; mp 140−142 °C; ^{1}H NMR (700 MHz, $CDCl_3$) δ: 7.88 (d, 2H, J = 8.8 Hz), 7.79 (d, 1H, J = 7.6 Hz), 7.64−7.62 (m, 1H), 7.31 (d, 1H, J = 8.3 Hz), 7.20 (t, 1H, J = 7.5 Hz), 6.97 (d, 2H, J = 8.8 Hz), 6.88 (s, 1H), 3.86 (s, 3H); ^{13}C NMR (700 MHz, $CDCl_3$) δ: 184.5, 165.8, 161.1, 145.9, 136.5, 133.4, 125.0, 124.5, 123.3, 121.9, 114.5, 113.4, 112.9, 55.4; HRMS $[M - H]^+$ calcd for $C_{16}H_{12}O_3$ 251.0708, found 251.0701.

*2-[(3′,4′-Dimethoxyphenyl)methylidene]-2,3-dihydro-1-benzofuran-3-one (**MA3**).* Quantitative yield, yellow solid; mp 157−159 °C; ^{1}H NMR (700 MHz, $CDCl_3$) δ: 7.81 (d, 1H, J = 7.5 Hz), 7.66−7.63 (m, 1H), 7.54 (d, 1H, J = 1.7 Hz), 7.50 (dd, 1H, J = 8.4, 1.7 Hz), 7.31 (d, 1H, J = 8.3 Hz), 7.22 (t, 1H, J = 7.4 Hz), 6.95 (d, 1H, J = 8.3 Hz), 6.87 (s, 1H), 3.98 (s, 3H), 3.95 (s, 3H); ^{13}C NMR (700 MHz, $CDCl_3$) δ: 184.5, 165.8, 150.9, 149.1, 146.0, 136.6, 126.1, 125.3, 124.6, 123.4, 122.0, 113.8, 113.7, 112.9, 111.3, 56.0 (2); HRMS $[M - H]^-$ calcd for $C_{17}H_{14}O_4$ 281.0814, found 281.0805.

*2-[(3′,5′-Dimethoxyphenyl)methylidene]-2,3-dihydro-1-benzofuran-3-one (**MA4**).* 89.0% yield, yellow solid; mp 157−160 °C; ^{1}H NMR (400 MHz, $CDCl_3$) δ: 7.78 (d, 1H J = 7.2 Hz), 7.66−7.62 (m, 1H), 7.30 (d, 1H, J = 8.3 Hz), 7.20 (t, 1H, J = 7.5 Hz), 7.07 (s, 1H), 7.06 (s, 1H), 6.79 (s, 1H), 6.51 (t, 1H, J = 2.2 Hz), 3.84 (s, 6H); ^{13}C NMR (400 MHz, $CDCl_3$) δ: 184.8, 166.2, 160.9, 147.1, 137.1, 133.9, 124.8, 123.6, 121.7, 113.1, 113.0, 109.6, 102.4, 55.6; HRMS $[M + H]^+$ calcd for $C_{17}H_{14}O_4$ 283.0970, found 283.0979.

*2-[(2′,4′,5′-Trimethoxyphenyl)methylidene]-2,3-dihydro-1-benzofuran-3-one (**MA5**).* 99.0% yield, yellow solid; mp 240−242 °C; ^{1}H NMR (700 MHz, $CDCl_3$) δ: 7.91 (s, 1H), 7.80 (dd, 1H, J = 7.6, 7.0 Hz), 7.63−7.61 (m, 1H), 7.46 (s, 1H), 7.28 (d, 1H, J = 8.2 Hz), 7.20 (t, 1H, J = 7.6 Hz), 6.51 (s, 1H), 3.96 (s, 3H), 3.95 (s, 3H), 3.90 (s, 3H); ^{13}C NMR (700 MHz, $CDCl_3$) δ: 184.3, 165.4, 155.3, 152.4, 145.7, 143.2, 136.2, 124.5, 123.2, 122.2, 114.5, 113.1, 112.8, 108.0, 96.3, 56.6, 56.4, 56.0; HRMS calcd for $C_{18}H_{16}O_5$ 312.0998, found 312.0998.

*2-[(3′,4′,5′-Trimethoxyphenyl)methylidene]-2,3-dihydro-1-benzofuran-3-one (**MA6**).* 89.0%, yellow solid; mp 182−183 °C; ^{1}H NMR (700 MHz, $CDCl_3$) δ: 7.82 (d, 1H, J = 7.2 Hz), 7.68−7.63 (m, 1H), 7.31 (d, 1H, J = 8.3 Hz), 7.24 (t, 1H, J = 7.4 Hz), 7.19 (s, 2H), 6.84 (s, 1H), 3.95 (s, 6H), 3.93 (s, 3H); ^{13}C NMR (700 MHz, $CDCl_3$) δ: 184.5, 165.9, 153.3, 146.4, 140.1, 136.8, 127.7, 124.7, 123.5, 121.7, 113.4, 112.9, 108.9, 61.0, 56.2; HRMS $[M + H]^+$ calcd for $C_{18}H_{16}O_5$ 313.1076, found 313.1082

General Procedure for the Synthesis of Hydroxyaurones (HA2−6). Methoxyaurone **MA2−6** (0.25 mmol, 1.0 equiv) was dissolved in anhydrous CH_2Cl_2 (15 mL) and cooled to 0 °C. BBr_3 (1 mmol, 4.0 equiv) was added slowly to the reaction mixture under N_2 atmosphere and stirred. The reaction mixture was allowed to attain room temperature and stirring continued for 12 h. TLC examination (50% EtOAc in hexanes) revealed the completion of the reaction. The reaction mixture was then cooled to 0 °C and carefully quenched with slow dropwise addition of water until the excess BBr_3 reacted completely. The precipitated solid product was filtered, washed with water, and dried over $CaCl_2$ in a vacuum desiccator. The crude product thus obtained was purified by column chromatography over Si gel using 10% MeOH in CH_2Cl_2 to afford pure hydroxyl aurones **HA2−6**. All hydroxyaurones were characterized by ^{1}H NMR, ^{13}C NMR, and HRMS as follows.

*2-[(4′-Hydroxyphenyl)methylidene]-2,3-dihydro-1-benzofuran-3-one (**HA2**).* 89.8% yield, yellow solid; mp 264−266 °C; ^{1}H NMR (700 MHz, DMSO-d_6) δ: 10.23 (s, 1H), 7.88 (d, 2H, J = 8.4 Hz), 7.79−7.77 (m, 2H), 7.54 (d, 1H, J = 8.6 Hz), 7.30 (t, 1H, J = 7.4 Hz), 6.91 (d, 3H, J = 8.8 Hz); ^{13}C NMR (700 MHz, DMSO-d_6) δ: 183.2, 165.0, 159.8, 144.7, 137.2, 133.8, 124.1, 123.7, 122.9, 121.3, 116.2, 113.5, 113.2; HRMS $[M + H]^+$ calcd for $C_{15}H_{10}O_3$ 239.0708, found 239.0718.

*2-[(3′,4′-Dihydroxyphenyl)methylidene]-2,3-dihydro-1-benzofuran-3-one (**HA3**).* 92.0% yield, yellow solid; mp 231−233 °C; ^{1}H NMR (400 MHz, DMSO-d_6) δ: 9.82 (bs, 1H), 9.34 (bs, 1H), 7.80−7.76 (m, 2H), 7.53−7.50 (m, 2H), 7.34−7.28 (m, 2H), 6.86 (d, 1H), 6.82 (s, 1H); ^{13}C NMR (700 MHz, DMSO-d_6) δ: 183.1, 165.0, 148.6, 145.7, 144.7, 137.1, 125.2, 124.1, 123.7, 123.3, 121.4, 118.3 (d), 116.1 (d), 114.0 (d), 113.0; HRMS $[M + H]^+$ calcd for $C_{15}H_{10}O_4$ 255.0657, found 255.0660.

*2-[(3′,5′-Dihydroxyphenyl)methylidene]-2,3-dihydro-1-benzofuran-3-one (**HA4**).* 80.0% yield, gray solid; decomposed at 250 °C; ^{1}H NMR (700 MHz, DMSO-d_6) δ: 7.79 (t, 2H, J = 7.4 Hz), 7.50 (d, 1H, J = 8.6 Hz), 7.30 (t, 1H, J = 7.3 Hz), 6.88 (d, 2H, J = 2.3 Hz), 6.73 (s, 1H), 6.36 (t, 1H, J = 2.0 Hz); ^{13}C NMR (700 MHz, DMSO-d_6) δ: 183.7, 165.4, 158.7, 146.2, 137.8, 133.2, 124.4, 124.0, 121.0, 113.1, 113.1, 109.7, 105.0; HRMS $[M - H]^-$ calcd for $C_{15}H_{10}O_4$ 253.0501, found 253.0513.

*2-[(2′,4′,5′-Trihydroxyphenyl)methylidene]-2,3-dihydro-1-benzofuran-3-one (**HA5**).* 83.0% yield, red solid; mp 191−193 °C; ^{1}H NMR (400 MHz, acetone-d_6) δ: 8.94 (s, 1H), 8.71 (s, 1H), 7.97 (s, 1H), 7.85 (s, 1H), 7.71−7.76 (m, 2H), 7.43 (d, 1H, J = 8.2 Hz), 7.40 (s, 1H), 7.28 (t, 1H, J = 7.4 Hz), 6.57 (s, 1H); ^{13}C NMR (400 MHz, acetone-d_6) δ: 183.9, 166.1, 153.8, 150.7, 145.6, 139.7, 137.2, 124.7, 124.1, 123.0, 117.7, 113.7, 111.6, 108.9, 103.7; HRMS calcd for $C_{15}H_{10}O_5$ 270.0528, found 270.0529.

*2-[(3′,4′,5′-Trihydroxyphenyl)methylidene]-2,3-dihydro-1-benzofuran-3-one (**HA6**).* 86.0% yield, greenish-yellow solid; decomposed at 256 °C; ^{1}H NMR (700 MHz, DMSO-d_6) δ: 9.28 (s, 2H), 9.05 (s, 1H), 7.78−7.76 (m, 2H), 7.48 (d, 1H, J = 8.5 Hz), 7.28 (dd, 1H, J = 14.8, 7.3 Hz), 7.03 (s, 2H), 6.72 (s, 1H); ^{13}C NMR (700 MHz, DMSO-d_6) δ: 183.0, 164.9, 146.2, 144.8, 137.1, 137.0, 124.2, 123.7, 122.0, 121.4, 114.5, 113.0, 111.3; HRMS $[M - H]^-$ calcd for $C_{15}H_{10}O_5$ 269.0450, found 269.0445.

Biofilm Inhibition Assays. Biofilm inhibition assays were performed in polystyrene microtiter 96-well plates. Stock solutions were prepared in a chemically defined medium (CDM, JRH Biosciences, Lenexa, KS) with 1% sucrose, 1% bacteria cultures and various concentrations of the small-molecule inhibitors to examine their activity against biofilm formation as described.[69,70] These stocks were assayed in 96-well plates in triplicate and incubated at 37 °C and 5% CO_2 for 16 h. After reading optical density for bacterial growth, the plate was gently washed with water, dried, and stained with crystal violet, and then gently rinsed again with deionized water leaving the stained biofilm at the bottoms of the wells. Biofilms were dissolved in 200 μL of 30% acetic acid and absorbance at 562 nm was read to determine the biofilm biomass. Each assay was carried out at least in triplicate. Biofilm inhibitory concentration (IC_{50}) of the compounds was determined by serial dilutions.

Gtf Inhibition Determined by Glucan Quantification Assays. Overnight cultures of *S. mutans* UA159 were centrifuged (6500 rpm, 4 °C, 10 min) to remove cells. The supernatant was mixed with ethanol (1:1) and incubated at −80 °C for 1 h. The precipitated Gtfs were palleted using centrifugation and resuspended in chemically defined media (CDM). 10 μL of Gtfs suspended in CDM was assayed on Ibidi slides with varying concentrations of inhibitor, 1% sucrose, 1% DMSO, and 1 μM Cascade blue dye in CDM. The slides were then incubated at 37 °C with 5% CO_2 for 16 h after which the wells of Ibidi slides were gently rinsed with 1× PBS and treated with 1× PBS for fluorescence microscopy imaging. The images obtained were processed in ImageJ to quantify glucans and graphed in GraphPad Prism.

***S. mutans*, *S. gordonii*, and *S. sanguinis* Growth Assays.** Effects of compounds on *S. mutans* and commensal bacterial growth were evaluated using the growth assay as described.[69] *S. mutans* UA159, *S. gordonii* DL1, and *S. sanguinis* SK36 cultures were grown for 24 h under 5% CO_2 at 37 °C. These cultures were then reinoculated with fresh THB (1:5) until OD_{470} = 1 when the bacteria were ready to be used. Different concentrations of the inhibitor were assayed in chemically defined media (CDM) with 1% bacteria, 1%

https://doi.org/10.1021/acs.jmedchem.3c00272
J. Med. Chem. 2023, 66, 7909−7925

sucrose, and 1% DMSO in 96-well plates. The 96-well plates were incubated under 5% CO_2 at 37 °C for 16 h. Growth of the bacteria was read after 16 h at OD_{470}. Each assay was carried out at least in triplicate.

Synthesis of Porous Cubic Manganese Oxide Microparticle Templates. Porous Mn_2O_3 microparticle templates of 3 μm in size were synthesized as described previously.[63,65] Briefly, a nanoseed solution was prepared by mixing 0.04 g NH_4HCO_3 and 0.02 g $MnSO_4$ in DI water (200 mL). Then, the nanoseed solution (80 mL) was added to 6 mM $MnSO_4$ (1000 mL), containing 2-propanol (0.5% vol), followed by the addition of 6 mM solution of NH_4HCO_3 (1000 mL), containing 2-propanol (0.5% vol) and the solution and was heated at 60 °C for 30 min to produce 3 μm cubic manganese carbonate particles. Once collected and dried via filtration, the $MnCO_3$ microparticles were heated at 650 °C for 3.5 h in a muffled oven to produce porous Mn_2O_3 microparticles.

Synthesis of Cubical Hydrogel Microparticles. pH-responsive cubic hydrogel microparticles were synthesized by depositing hydrogen-bonded $(PMAA/PVPON)_n$ (the subscript denotes the number of polymer bilayers) multilayers at the surfaces of Mn_2O_3 microparticle templates. The porous templates were first exposed to an aqueous poly(ethyleneimine) (PEI) solution in deionized (DI) water (1.5 mg/mL) for 1 h to enhance the adsorption of the following (PMAA/PVPON) layers to the particle surfaces followed by deposition of the polymers from aqueous polymeric solutions (1.5 mg/mL) at pH = 2 for 45 min each. The polymer deposition was achieved through sonication (15 min) and shaking (30 min) of the manganese oxide porous templates in polymer solutions. After the deposition of each layer, the template particles were centrifuged for 10 min at 4900 rpm and resuspended in phosphate buffer solution (0.01 M, pH = 2) twice to rinse away excess polymer before the next deposition cycle. Following the deposition of a five-bilayer $(PMAA/PVPON)_5$ coating, the PMAA layers were cross-linked with ethylenediamine by, first, activating the PMAA carboxylic groups with a carbodiimide solution (5 mg/mL, pH = 5, 0.01 M phosphate) for 30 min, then exposing the particles to ethylenediamine (12 μL/mL in 0.01 M phosphate, pH = 5.8) for 16 h. Afterward, PVPON was removed from the PMAA network by exposing the core−shell particles to 0.01 M phosphate buffer solution (pH = 8.5) for 24 h while shaking. Cubic PMAA hydrogel microparticles were obtained after dissolving the manganese oxide core in hydrochloric acid solution (8M HCl) for 24 h. The hydrogel microparticles were treated with ethylenediamine tetraacetic acid disodium salt solution (EDTA, 0.1 M) at pH = 7 overnight by shaking to remove any residual manganese ions in the hydrogel network. The PMAA hydrogel microparticles were then purified by dialysis in DI water for 3 days using a Float-a-Lyzer (Fisher; MWCO 20 kDa).

Rat Model of Dental Caries. *In vivo* studies of colonization and virulence of *S. mutans* were evaluated using a previously reported rat model of dental caries.[71] Offspring of gnotobiotic Fischer 344 rats used in this experiment were bred and maintained in trexler isolators. Male and female rat pups were removed from isolators at 20 days of age and randomly assigned into five treatment groups of five rats/group in cages with filter tops. Rats were then infected with *S. mutans* UA159 strain by oral swabbing daily for 4 consecutive days with a fresh overnight culture of *S. mutans* UA159. Rats were provided with caries promoting Teklad Diet 305 containing 5% sucrose (Harlan Laboratories, Inc., Indianapolis, IN) and sterile drinking water *ad libitum*. Oral swabs were taken 5 days post-infection and plated on Todd Hewitt (TH) agar plates and incubated at 37 °C in an environment of 5% CO_2 in the air to confirm colonization. Rats were weighed at weaning and at the termination of the experiment. One-week post-infection, the molars of the rats were treated topically twice daily for 4 weeks with the test compounds using camel-hair brushes. The five treatment groups used in this study were (1) **HEBI** (100 μM); (2) **HA5** (100 μM); (3) hydrogel-encapsulated PBS (no drug) containing 0.1% DMSO (negative control), (4) 250 ppm NaF (positive control), and (5) infected untreated group (negative control). Drinking water was withheld for 60 min following each treatment with the compound. Animals were weighed at weaning and at the termination of the experiment. On day 60, the rats were sacrificed using CO_2 followed by cervical dislocation or bilateral thoracotomy. The mandibles were surgically removed and cleaned of excess tissue to assess the level of bacteria present and the extent of caries formation. The right mandibles from each rat were placed in a tube containing phosphate buffer (3 mL), placed on ice and sonicated (10 s) to release bacteria from the molars. Each sample was serially diluted, plated on blood agar plates (BAP) and mitis salivarius (MS) agar plates, and incubated in an environment of 5% CO_2 at 37 °C to quantify the level of total bacteria and *S. mutans* present in the plaque. The right and left mandibles from each rat were then placed in 95% ethanol for 24 h. The mandibles were cleaned and stained overnight with murexide solution. After drying, the mandibles were sectioned and scored for caries activity using the Keyes method.[68] Caries scores were recorded for the buccal, sulcal, and proximal molar surfaces individually so that differences among the surfaces can be distinguished. Statistical significance in the mean caries scores, colony-forming units (CFUs)/mandible, and body weights between groups of rats were determined by one-way analysis of variance (ANOVA) with the Tukey−Kramer multiple comparison test using the InStat program (Graphpad Software, San Diego, CA). When determining the statistical significance between the two groups, an unpaired *t*-test was applied. Differences between groups were considered significant at a *P*-value < 0.05. All experimental protocols were approved by the University of Alabama at Birmingham Institutional Animal Care and Use Committee (Protocol No. IACUC-20047). The methods were carried out in accordance with the relevant guidelines and regulations.

■ ASSOCIATED CONTENT

Supporting Information

The Supporting Information is available free of charge at https://pubs.acs.org/doi/10.1021/acs.jmedchem.3c00272.

Molecular formula strings (CSV)

Copies of ^{1}H NMR and ^{13}C NMR spectra and HPLC traces for all compounds evaluated and coordinates for the HA5/GtfB cocrystal structure are deposited in the protein data bank (8FG8) (PDF)

■ AUTHOR INFORMATION

Corresponding Authors

Hui Wu − *Department of Integrative Biomedical and Diagnostic Sciences, Oregon Health and Science University, Portland, Oregon 97239, United States*; Phone: 503-418-2090; Email: wuhu@ohsu.edu

Eugenia Kharlampieva − *Department of Chemistry and Center of Nanoscale Materials and Biointegration, University of Alabama at Birmingham, Birmingham, Alabama 35294, United States*; orcid.org/0000-0003-0227-0920; Phone: (205) 975-8288; Email: ekharlam@uab.edu

Sadanandan E. Velu − *Department of Chemistry and Microbiome Center, University of Alabama at Birmingham, Birmingham, Alabama 35294, United States*; orcid.org/0000-0002-0342-2378; Phone: (205) 975-2478; Email: svelu@uab.edu

Authors

Parmanand Ahirwar − *Department of Chemistry, University of Alabama at Birmingham, Birmingham, Alabama 35294, United States*

Veronika Kozlovskaya − *Department of Chemistry, University of Alabama at Birmingham, Birmingham, Alabama 35294, United States*; orcid.org/0000-0001-9089-4842

https://doi.org/10.1021/acs.jmedchem.3c00272
J. Med. Chem. 2023, 66, 7909−7925

Bhavitavya Nijampatnam − *Department of Chemistry, University of Alabama at Birmingham, Birmingham, Alabama 35294, United States*
Edwin M. Rojas − *Department of Chemistry and School of Dentistry, University of Alabama at Birmingham, Birmingham, Alabama 35294, United States*
Piyasuda Pukkanasut − *Department of Chemistry, University of Alabama at Birmingham, Birmingham, Alabama 35294, United States*
Daniel Inman − *Department of Chemistry, University of Alabama at Birmingham, Birmingham, Alabama 35294, United States*
Maksim Dolmat − *Department of Chemistry, University of Alabama at Birmingham, Birmingham, Alabama 35294, United States;* orcid.org/0000-0002-4918-7342
Anna C. Law − *Department of Chemistry, University of Alabama at Birmingham, Birmingham, Alabama 35294, United States*
Norbert Schormann − *Department of Biochemistry and Molecular Genetics, University of Alabama at Birmingham, Birmingham, Alabama 35294, United States*
Champion Deivanayagam − *Department of Biochemistry and Molecular Genetics, University of Alabama at Birmingham, Birmingham, Alabama 35294, United States*
Gregory J. Harber − *Department of Microbiology, University of Alabama at Birmingham, Birmingham, Alabama 35294, United States*
Suzanne M. Michalek − *Department of Microbiology, University of Alabama at Birmingham, Birmingham, Alabama 35294, United States*

Complete contact information is available at: https://pubs.acs.org/10.1021/acs.jmedchem.3c00272

Author Contributions

○P.A. and V.K. contributed equally to this manuscript. S.E.V., E.K., and H.W.: conceived the idea and designed the experiments; P.A., V.K., B.N., E.M.R., P.P., D.I., M.D., A.C.L., N.S., C.D., G.H., and S.M.M.: performed the experiments; P.A., and S.E.V.: drafted and finalized the manuscript.

Notes

The authors declare no competing financial interest.
All compounds are >95% pure by HPLC analysis.

■ ACKNOWLEDGMENTS

The contents described in this report were supported by the National Institute of Dental and Craniofacial Research, the National Institutes of Health Grants R21DE028349 (Velu), R03DE025058 (Velu), R01DE022350 (Wu), F31DE025783 (Nijampatnam), and F30DE030334 (Rojas), and the University of Alabama at Birmingham Microbiome Center Pilot Grant (Velu). This work was also supported by NSF DMR Award No. 1904816 (Kharlampieva). The authors thank Dr. Nathaniel Lawson (UAB School of Dentistry) for the generous supply of freshly extracted, intact third molars with flat surfaces (IRB-300001291) used in this study.

■ ABBREVIATIONS USED

AFM, atomic force microscope; BOC, *tert*-butyloxy carbonyl; BrS, broad signal; CDM, chemically defined medium; CFU, colony-forming unit; DMAP, *N*,*N*-dimethyl aminopyridine; DMSO, dimethyl sulfoxide; EDC, *N*-ethyl-*N*′-(3-dimethylaminopropyl)carbodiimide; EPS, extracellular polysaccharide; Gtf, glucosyltransferases; HEBI, hydrogel-encapsulated biofilm inhibitor; HRMS, high-resolution mass spectrometry; IC_{50}, half-maximal inhibitory concentration; LC-MS, liquid-chromatography mass spectrometry; NMR, nuclear magnetic resonance; SAR, structure−activity relationship; SDS-PAGE, sodium dodecyl sulfate−polyacrylamide gel electrophoresis; S. gordonii, Streptococcus gordonii; S. mutans, Streptococcus mutans; S. sanguinis, Streptococcus sanguinis; TFA, trifluoroacetic acid; THB, Todd Hewitt Broth

■ REFERENCES

(1) Marsh, P. D. Dental Plaque as a Microbial Biofilm. *Caries Res.* **2004**, *38*, 204−211.
(2) Vos, T.; Allen, C.; Arora, M.; Barber, R. M.; Bhutta, Z. A.; Brown, A.; Carter, A.; Casey, D. C.; Charlson, F. J.; Chen, A. Z.; Coggeshall, M.; Cornaby, L.; Dandona, L.; Dicker, D. J.; Dilegge, T.; Erskine, H. E.; Ferrari, A. J.; Fitzmaurice, C.; Fleming, T.; Murray, C. J. L.; et al. Global, Regional, and National Incidence, Prevalence, and Years Lived with Disability for 310 Diseases and Injuries, 1990-2015: A Systematic Analysis for the Global Burden of Disease Study 2015. *Lancet* **2016**, *388*, 1545−1602.
(3) (a) Banas, J. A.; Vickerman, M. M. Glucan-binding Proteins of the Oral Streptococci. *Crit. Rev. Oral Biol. Med.* **2003**, *14*, 89−99. (b) Kim, J. K.; Baker, L. A.; Davarian, S.; Crimmins, E. Oral Health Problems and Mortality. *J. Dent. Sci.* **2013**, *8*, 115−120.
(4) (a) Hamada, S.; Slade, H. D. Biology, Immunology, and Cariogenicity of *Streptococcus mutans*. *Microbiol. Rev.* **1980**, *44*, 331−384. (b) Loesche, W. J. Role of *Streptococcus mutans* in Human Dental Decay. *Microbiol. Rev.* **1986**, *50*, 353−380.
(5) Overman, P. R. Biofilm: A New View of Plaque. *J. Contemp. Dent. Pract.* **2000**, *1*, 37−44.
(6) (a) Ahovuo-Saloranta, A.; Forss, H.; Walsh, T.; Nordblad, A.; Mäkelä, M.; Worthington, H. V. Pit and Fissure Sealants for Preventing Dental Decay in Permanent Teeth. *Cochrane Database Syst. Rev.* **2017**, *2017*, No. CD001830. (b) Baik, A.; Alamoudi, N.; El-Housseiny, A.; Altuwirqi, A. Fluoride Varnishes for Preventing Occlusal Dental Caries: A Review. *Dent. J.* **2021**, *9*, No. 64.
(7) (a) Aoun, A.; Darwiche, F.; Al Hayek, S.; Doumit, J. The Fluoride Debate: The Pros and Cons of Fluoridation. *Prev. Nutr. Food Sci.* **2018**, *23*, 171−180. (b) Duffin, S.; Duffin, M.; Grootveld, M. Revisiting Fluoride in the Twenty First Century: Safety and Efficacy Considerations. *Front. Oral Health* **2022**, *3*, No. 873157.
(8) Grandjean, P. Developmental Fluoride Neurotoxicity: An Updated Review. *Environ. Health* **2019**, *18*, No. 110.
(9) Oyanagi, T.; Tagami, J.; Matin, K. Potentials of Mouthwashes in Disinfecting Cariogenic Bacteria and Biofilms Leading to Inhibition of Caries. *Open Dent. J.* **2012**, *6*, 23−30.
(10) Kolenbrander, P. E. Oral Microbial Communities: Biofilms, Interactions, and Genetic Systems. *Annu. Rev. Microbiol.* **2000**, *54*, 413−437.
(11) (a) Ren, Z.; Chen, L.; Li, J.; Li, Y. Inhibition of *Streptococcus mutans* Polysaccharide Synthesis by Molecules Targeting Glycosyltransferase Activity. *J. Oral Microbiol.* **2016**, *8*, No. 31095. (b) Ren, Z.; Cui, T.; Zeng, J.; Chen, L.; Zhang, W.; Xu, X.; Cheng, L.; Li, M.; Li, J.; Zhou, X.; Li, Y. Molecule Targeting Glucosyltransferase Inhibits *Streptococcus mutans* Biofilm Formation and Virulence. *Antimicrob. Agents Chemother.* **2016**, *60*, 126−135. (c) Taubman, M. A.; Nash, D. A. The Scientific and Public Health Imperative for a Vaccine Against Dental Caries. *Nat. Rev. Immunol.* **2006**, *6*, 555−563.
(12) Koo, H.; Jeon, J. G. Naturally Occurring Molecules as Alternative Therapeutic Agents Against Cariogenic Biofilms. *Adv. Dent. Res.* **2009**, *21*, 63−68.
(13) (a) Jenkinson, H. F.; Lamont, R. J. Oral Microbial Communities in Sickness and in Health. *Trends Microbiol.* **2005**, *13*, 589−595. (b) Kolenbrander, P. E.; Andersen, R. N.; Blehert, D. S.; Egland, P. G.; Foster, J. S.; Palmer, R. J., Jr. Communication Among Oral Bacteria. *Microbiol. Mol. Biol. Rev.* **2002**, *66*, 486−505.

(c) Kuramitsu, H. K.; He, X.; Lux, R.; Anderson, M. H.; Shi, W. Interspecies Interactions Within Oral Microbial Communities. *Microbiol. Mol. Biol. Rev.* **2007**, *71*, 653−670.
(14) (a) Bowden, G. H.; Hamilton, I. R. Survival of Oral Bacteria. *Crit. Rev. Oral Biol. Med.* **1998**, *9*, 54−85. (b) Quivey, R. G., Jr.; Kuhnert, W. L.; Hahn, K.Adaptation of Oral Streptococci to Low pH. In *Advances in Microbial Physiology*; Elsevier, 2000; Vol. *42*, pp 239−274.
(15) Matsumoto-Nakano, M. Role of *Streptococcus mutans* Surface Proteins for Biofilm Formation. *Jpn. Dent. Sci. Rev.* **2018**, *54*, 22−29.
(16) Yamashita, Y.; Bowen, W. H.; Burne, R. A.; Kuramitsu, H. K. Role of the *Streptococcus mutans* gtf Genes in Caries Induction in the Specific Pathogen-free Rat Model. *Infect. Immun.* **1993**, *61*, 3811−3817.
(17) (a) Aoki, H.; Shiroza, T.; Hayakawa, M.; Sato, S.; Kuramitsu, H. K. Cloning of a *Streptococcus mutans* Glucosyltransferase Gene Coding for Insoluble Glucan Synthesis. *Infect. Immun.* **1986**, *53*, 587−594. (b) Hanada, N.; Kuramitsu, H. K. Isolation and Characterization of the *Streptococcus mutans* gtfC Gene Coding for Synthesis of Both Soluble and Insoluble Glucans. *Infect. Immun.* **1988**, *56*, 1999−2005.
(18) (a) Hanada, N.; Kuramitsu, H. K. Isolation and Characterization of the *Streptococcus mutans* gtfD Gene Coding for Primer-dependent Soluble Glucan Synthesis. *Infect. Immun.* **1989**, *57*, 2079−2085. (b) Monchois, V.; Willemot, R. M.; Monsan, P. Glucansucrases: Mechanism of Action and Structure-function Relationships. *FEMS Microbiol. Rev.* **1999**, *23*, 131−151.
(19) Nijampatnam, B.; Ahirwar, P.; Pukkanasut, P.; Womack, H.; Casals, L.; Zhang, H.; Cai, X.; Michalek, S. M.; Wu, H.; Velu, S. E. Discovery of Potent Inhibitors of *Streptococcus mutans* Biofilm with Antivirulence Activity. *ACS Med. Chem. Lett.* **2021**, *12*, 48−55.
(20) (a) Nijampatnam, B.; Casals, L.; Zheng, R.; Wu, H.; Velu, S. E. Hydroxychalcone Inhibitors of *Streptococcus mutans* Glucosyl transferases and Biofilms as Potential Anticaries Agents. *Bioorg. Med. Chem. Lett.* **2016**, *26*, 3508−3513. (b) Nijampatnam, B.; Zhang, H.; Cai, X.; Michalek, S. M.; Wu, H.; Velu, S. E. Inhibition of *Streptococcus mutans* Biofilms by the Natural Stilbene Piceatannol Through the Inhibition of Glucosyltransferases. *ACS Omega* **2018**, *3*, 8378−8385.
(21) Zhang, Q.; Nijampatnam, B.; Hua, Z.; Nguyen, T.; Zou, J.; Cai, X.; Michalek, S. M.; Velu, S. E.; Wu, H. Structure-Based Discovery of Small Molecule Inhibitors of Cariogenic Virulence. *Sci. Rep.* **2017**, *7*, No. 5974.
(22) Girón, C. B. T.; Sierra, J. F. H.; DeAlba-Montero, I.; de los A Urbano Peña, M.; Ruiz, F. Therapeutic Use of Silver Nanoparticles in the Prevention and Arrest of Dental Caries. *Bioinorg. Chem. Appl.* **2020**, *2020*, 1−7.
(23) Sims, K. R.; Maceren, J. P.; Liu, Y.; Rocha, G. R.; Koo, H.; Benoit, D. S. W. Dual Antibacterial Drug-loaded Nanoparticles Synergistically Improve Treatment of *Streptococcus mutans* Biofilms. *Acta Biomater.* **2020**, *115*, 418−431.
(24) (a) Horev, B.; Klein, M. I.; Hwang, G.; Li, Y.; Kim, D.; Koo, H.; Benoit, D. S. pH-activated nanoparticles for controlled topical delivery of farnesol to disrupt oral biofilm virulence. *ACS Nano* **2015**, *9*, 2390−2404. (b) Yi, Y.; Wang, L.; Chen, L.; Lin, Y.; Luo, Z.; Chen, Z.; Li, T.; Wu, J.; Zhong, Z. Farnesal-loaded pH-Sensitive Polymeric Micelles Provided Effective Prevention and Treatment on Dental Caries. *J. Nanobiotechnol.* **2020**, *18*, No. 89.
(25) Jailani, A.; Kalimuthu, S.; Rajasekar, V.; Ghosh, S.; Collart-Dutilleul, P. Y.; Fatima, N.; Koo, H.; Solomon, A. P.; Cuisinier, F.; Neelakantan, P. Trans-Cinnamaldehyde Eluting Porous Silicon Microparticles Mitigate Cariogenic Biofilms. *Pharmaceutics* **2022**, *14*, No. 1428.
(26) (a) Liu, Y.; Huang, Y.; Kim, D.; Ren, Z.; Oh, M. J.; Cormode, D. P.; Hara, A. T.; Zero, D. T.; Koo, H. Ferumoxytol Nanoparticles Target Biofilms Causing Tooth Decay in the Human Mouth. *Nano Lett.* **2021**, *21*, 9442−9449. (b) Liu, Y.; Naha, P. C.; Hwang, G.; Kim, D.; Huang, Y.; Simon-Soro, A.; Jung, H. I.; Ren, Z.; Li, Y.; Gubara, S.; Alawi, F.; Zero, D.; Hara, A. T.; Cormode, D. P.; Koo, H. Topical Ferumoxytol Nanoparticles Disrupt Biofilms and Prevent Tooth Decay In Vivo via Intrinsic Catalytic Activity. *Nat. Commun.* **2018**, *9*, No. 2920.
(27) Melo, M. A.; Guedes, S. F.; Xu, H. H.; Rodrigues, L. K. Nanotechnology-based Restorative Materials for Dental Caries Management. *Trends Biotechnol.* **2013**, *31*, 459−467.
(28) Mohire, N. C.; Yadav, A. V. Chitosan-based Polyherbal Toothpaste: As Novel Oral Hygiene Product. *Indian J. Dent. Res.* **2010**, *21*, 380−384.
(29) (a) Seneviratne, C. J.; Leung, K. C.-F.; Wong, C.-H.; Lee, S.-F.; Li, X.; Leung, P. C.; Lau, C. B. S.; Wat, E.; Jin, L. Nanoparticle-Encapsulated Chlorhexidine against Oral Bacterial Biofilms. *PLoS One* **2014**, *9*, No. e103234. (b) Zhang, J. F.; Wu, R.; Fan, Y.; Liao, S.; Wang, Y.; Wen, Z. T.; Xu, X. Antibacterial Dental Composites with Chlorhexidine and Mesoporous Silica. *J. Dent. Res.* **2014**, *93*, 1283−1289.
(30) Nguyen, S.; Hiorth, M.; Rykke, M.; Smistad, G. Polymer Coated Liposomes for Dental Drug Delivery: Interactions with Parotid Saliva and Dental Enamel. *Eur. J. Pharm. Sci.* **2013**, *50*, 78−85.
(31) Feitosa, S. A.; Palasuk, J.; Kamocki, K.; Geraldeli, S.; Gregory, R. L.; Platt, J. A.; Windsor, L. J.; Bottino, M. C. Doxycycline-Encapsulated Nanotube-Modified Dentin Adhesives. *J. Dent. Res.* **2014**, *93*, 1270−1276.
(32) Zhou, Y.; Yang, J.; Lin, Z.; Li, J.; Liang, K.; Yuan, H.; Li, S.; Li, J. Triclosan-Loaded Poly(amido amine) Dendrimer for Simultaneous Treatment and Remineralization of Human Dentine. *Colloids Surf., B* **2014**, *115*, 237−243.
(33) Naha, P. C.; Liu, Y.; Hwang, G.; Huang, Y.; Gubara, S.; Jonnakuti, V.; Simon-Soro, A.; Kim, D.; Gao, L.; Koo, H.; Cormode, D. P. Dextran-Coated Iron Oxide Nanoparticles as Biomimetic Catalysts for Localized and pH-Activated Biofilm Disruption. *ACS Nano* **2019**, *13*, 4960−4971.
(34) (a) Aframian, D. J.; Davidowitz, T.; Benoliel, R. The Distribution of Oral Mucosal pH Values in Healthy Saliva Secretors. *Oral Dis.* **2006**, *12*, 420−423. (b) Baliga, S.; Muglikar, S.; Kale, R. Salivary pH: A Diagnostic Biomarker. *J. Indian Soc. Periodontol.* **2013**, *17*, 461−465.
(35) Lazarchik, D. A.; Filler, S. J. Effects of Gastroesophageal Reflux on the Oral Cavity. *Am. J. Med.* **1997**, *103*, 107S−113S.
(36) (a) Markitziu, A.; Aframian, D. Gastro-Intestinal Disorders. *Br. Dent. J.* **1997**, *182*, No. 207. (b) Robb, N. D.; Smith, B. G.; Geidrys-Leeper, E. The Distribution of Erosion in the Dentitions of Patients with Eating Disorders. *Br. Dent. J.* **1995**, *178*, 171−175.
(37) Meyer, F.; Enax, J.; Epple, M.; Amaechi, B. T.; Simader, B. Cariogenic Biofilms: Development, Properties, and Biomimetic Preventive Agents. *Dent. J.* **2021**, *9*, No. 88.
(38) Lawrence, N. J.; Rennison, D.; McGown, A. T.; Hadfield, J. A. The Total Synthesis of an Aurone Isolated from Uvaria hamiltonii: Aurones and Flavones as Anticancer Agents. *Bioorg. Med. Chem. Lett.* **2003**, *13*, 3759−3763.
(39) Ono, E.; Fukuchi-Mizutani, M.; Nakamura, N.; Fukui, Y.; Yonekura-Sakakibara, K.; Yamaguchi, M.; Nakayama, T.; Tanaka, T.; Kusumi, T.; Tanaka, Y. Yellow Flowers Generated by Expression of the Aurone Biosynthetic Pathway. *Proc. Natl. Acad. Sci. U.S.A.* **2006**, *103*, 11075−11080.
(40) Brooks, C. J. W.; Watson, D. G. Phytoalexins. *Nat. Prod. Rep.* **1985**, *2*, 427−459.
(41) Morimoto, M.; Fukumoto, H.; Nozoe, T.; Hagiwara, A.; Komai, K. Synthesis and Insect Antifeedant Activity of Aurones against Spodoptera litura Larvae. *J. Agric. Food Chem.* **2007**, *55*, 700−705.
(42) Okombi, S.; Rival, D.; Bonnet, S.; Mariotte, A. M.; Perrier, E.; Boumendjel, A. Discovery of Benzylidenebenzofuran-3(2H)-one (aurones) as Inhibitors of Tyrosinase Derived from Human Melanocytes. *J. Med. Chem.* **2006**, *49*, 329−333.
(43) Venkateswarlu, S.; Panchagnula, G. K.; Subbaraju, G. V. Synthesis and Antioxidative Activity of 3′,4′,6,7-Tetrahydroxyaurone, a Metabolite of Bidens frondosa. *Biosci. Biotechnol. Biochem.* **2004**, *68*, 2183−2185.
(44) (a) Ashok, D.; Rangu, K.; Gundu, S.; Lakkadi, A.; Tigulla, P. Microwave-Assisted Synthesis, Molecular Docking, and Biological

https://doi.org/10.1021/acs.jmedchem.3c00272
J. Med. Chem. 2023, 66, 7909−7925

Evaluation of 2-Arylidene-2H-furo[2,3-f]chromen-3(7H)-ones as Antioxidant and Antimicrobial Agents. *Med. Chem. Res.* **2017**, *26*, 1735−1746. (b) Campaniço, A.; Carrasco, M. P.; Njoroge, M.; Seldon, R.; Chibale, K.; Perdigao, J.; Portugal, I.; Warner, D. F.; Moreira, R.; Lopes, F. Azaaurones as Potent Antimycobacterial Agents Active against MDR- and XDR-TB. *Chem. Med. Chem.* **2019**, *14*, 1537−1546. (c) Jardosh, H. H.; Patel, M. P. Antimicrobial and Antioxidant Evaluation of New Quinolone Based Aurone Analogs. *Arabian J. Chem.* **2017**, *10*, S3781−S3791. (d) Kumar, G.; Lathwal, E.; Saroha, B.; Kumar, S.; Kumar, S.; Chauhan, N. S.; Kumar, T. Synthesis and Biological Evaluation of Quinoline-Based Novel Aurones. *ChemistrySelect* **2020**, *5*, 3539−3543. (e) Tiwari, K. N.; Monserrat, J.-P.; Hequet, A.; Ganem-Elbaz, C.; Cresteil, T.; Jaouen, G.; Vessières, A.; Hillard, E. A.; Jolivalt, C. In vitro Inhibitory Properties of FerroceneSubstituted Chalcones and Aurones on Bacterial and Human Cell Cultures. *Dalton Trans.* **2012**, *41*, 6451−6457.

(45) Balsera, B.; Mulet, J.; Fernández-Carvajal, A.; de la Torre-Martínez, R.; Ferrer-Montiel, A.; Hernández-Jiménez, J. G.; Estévez-Herrera, J.; Borges, R.; Freitas, A. E.; López, M. G.; García-López, M. T.; González-Muñiz, R.; de Vega, M. J. P.; Valor, L. M.; Svobodová, L.; Sala, S.; Sala, F.; Criado, M. Chalcones as Positive Allosteric Modulators of α7 Nicotinic Acetylcholine Receptors: A New Target for a Privileged Structure. *Eur. J. Med. Chem.* **2014**, *86*, 724−739.

(46) Stieger, N.; Liebenberg, W.; Wessels, J. C. UV Spectrophotometric Method for the Identification and Solubility Determination of Nevirapine. *Pharmazie* **2009**, *64*, 690−691.

(47) Mota, F. L.; Queimada, A. J.; Pinho, S. P.; Macedo, E. A. Aqueous Solubility of Some Natural Phenolic Compounds. *Ind. Eng. Chem. Res.* **2008**, *47*, 5182−5189.

(48) Lemos, J. A.; Abranches, J.; Koo, H.; Marquis, R. E.; Burne, R. A.Protocols to Study the Physiology of Oral Biofilms. In *Methods in Molecular Biology*; Springer, 2010; Vol. *666*, pp 87−102.

(49) (a) Koo, H.; Falsetta, M. L.; Klein, M. I. The Exopolysaccharide Matrix: A Virulence Determinant of Cariogenic Biofilm. *J. Dent. Res.* **2013**, *92*, 1065−1073. (b) Xiao, J.; Klein, M. I.; Falsetta, M. L.; Lu, B.; Delahunty, C. M.; Yates, J. R., 3rd; Heydorn, A.; Koo, H. The Exopolysaccharide Matrix Modulates the Interaction Between 3D Architecture and Virulence of a Mixed-Species Oral Biofilm. *PLoS Pathog.* **2012**, *8*, No. e1002623.

(50) Koo, H.; Xiao, J.; Klein, M. I.; Jeon, J. G. Exopolysaccharides Produced by *Streptococcus mutans* Glucosyltransferases Modulate the Establishment of Microcolonies Within Multispecies Biofilms. *J. Bacteriol.* **2010**, *192*, 3024−3032.

(51) Bowen, W. H.; Koo, H. Biology of *Streptococcus mutans* Derived Glucosyltransferases: Role in Extracellular Matrix Formation of Cariogenic Biofilms. *Caries Res.* **2011**, *45*, 69−86.

(52) (a) Huffines, J. T.; Scoffield, J. A. Disruption of *Streptococcus mutans* and *Candida albicans* Synergy by a Commensal *Streptococcus*. *Sci. Rep.* **2020**, *10*, No. 19661. (b) Huffines, J. T.; Stoner, S. N.; Baty, J. J.; Scoffield, J. A. Nitrite Triggers Reprogramming of the Oral Polymicrobial Metabolome by a Commensal *Streptococcus*. *Front. Cell Infect. Microbiol.* **2022**, *12*, No. 833339.

(53) (a) Kabsch, W. XDS. *Acta Crystallogr., Sect. D: Biol. Crystallogr.* **2010**, *66*, 125−132. (b) Kabsch, W. Integration, Scaling, Space-Group Assignment and Post-Refinement. *Acta Crystallogr., Sect. D: Biol. Crystallogr.* **2010**, *66*, 133−144.

(54) Evans, P. R. An Introduction to Data Reduction: Space-Group Determination, Scaling and Intensity Statistics. *Acta Crystallogr. D Biol. Crystallogr.* **2011**, *67*, 282−292.

(55) Winn, M. D.; Ballard, C. C.; Cowtan, K. D.; Dodson, E. J.; Emsley, P.; Evans, P. R.; Keegan, R. M.; Krissinel, E. B.; Leslie, A. G.; McCoy, A.; McNicholas, S. J.; Murshudov, G. N.; Pannu, N. S.; Potterton, E. A.; Powell, H. R.; Read, R. J.; Vagin, A.; Wilson, K. S. Overview of the CCP4 Suite and Current Developments. *Acta Crystallogr., Sect. D: Biol. Crystallogr.* **2011**, *67*, 235−242.

(56) Murshudov, G. N.; Vagin, A. A.; Dodson, E. J. Refinement of Macromolecular Structures by the Maximum-Likelihood Method. *Acta Crystallogr., Sect. D: Biol. Crystallogr.* **1997**, *53*, 240−255.

(57) (a) Afonine, P. V.; Grosse-Kunstleve, R. W.; Echols, N.; Headd, J. J.; Moriarty, N. W.; Mustyakimov, M.; Terwilliger, T. C.; Urzhumtsev, A.; Zwart, P. H.; Adams, P. D. Towards Automated Crystallographic Structure Refinement with Phenix.refine. *Acta Crystallogr., Sect. D: Biol. Crystallogr.* **2012**, *68*, 352−367. (b) Liebschner, D.; Afonine, P. V.; Baker, M. L.; Bunkóczi, G.; Chen, V. B.; Croll, T. I.; Hintze, B.; Hung, L. W.; Jain, S.; McCoy, A. J.; Moriarty, N. W.; Oeffner, R. D.; Poon, B. K.; Prisant, M. G.; Read, R. J.; Richardson, J. S.; Richardson, D. C.; Sammito, M. D.; Sobolev, O. V.; Stockwell, D. H.; Terwilliger, T. C.; Urzhumtsev, A. G.; Videau, L. L.; Williams, C. J.; Adams, P. D. Macromolecular Structure Determination Using X-rays, Neutrons and Electrons: Recent Developments in Phenix. *Acta Crystallogr., Sect. D: Struct. Biol.* **2019**, *75*, 861−877.

(58) Emsley, P.; Lohkamp, B.; Scott, W. G.; Cowtan, K. Features and Development of Coot. *Acta Crystallogr., Sect. D: Biol. Crystallogr.* **2010**, *66*, 486−501.

(59) Davies, G. J.; Wilson, K. S.; Henrissat, B. Nomenclature for Sugar-Binding Subsites in Glycosyl Hydrolases. *Biochem. J.* **1997**, *321*, 557−559.

(60) Zhang, Q.; Ma, Q.; Wang, Y.; Wu, H.; Zou, J. Molecular Mechanisms of Inhibiting Glucosyltransferases for Biofilm Formation in *Streptococcus mutans*. *Int. J. Oral Sci.* **2021**, *13*, No. 30.

(61) Cusack, K. P.; Arnold, L. D.; Barberis, C. E.; Chen, H.; Ericsson, A. M.; Gaza-Bulseco, G. S.; Gordon, T. D.; Grinnell, C. M.; Harsch, A.; Pellegrini, M.; Tarcsa, E. A 13C NMR Approach to Categorizing Potential Limitations of α,β-Unsaturated Carbonyl Systems in Drug-Like Molecules. *Bioorg. Med. Chem. Lett.* **2004**, *14*, 5503−5507.

(62) McGovern, S. L.; Helfand, B. T.; Feng, B.; Shoichet, B. K. A Specific Mechanism of Nonspecific Inhibition. *J. Med. Chem.* **2003**, *46*, 4265−4272.

(63) Kozlovskaya, V.; Chen, J.; Tedjo, C.; Liang, X.; Campos-Gomez, J.; Oh, J.; Saeed, M.; Lungu, C. T.; Kharlampieva, E. pH-Responsive Hydrogel Cubes for Release of Doxorubicin in Cancer Cells. *J. Mater. Chem. B* **2014**, *2*, 2494−2507.

(64) Xue, B.; Kozlovskaya, V.; Liu, F.; Chen, J.; Williams, J. F.; Campos-Gomez, J.; Saeed, M.; Kharlampieva, E. Intracellular Degradable Hydrogel Cubes and Spheres for Anti-Cancer Drug Delivery. *ACS Appl. Mater. Interfaces* **2015**, *7*, 13633−13644.

(65) Xue, B.; Wang, W.; Qin, J. J.; Nijampatnam, B.; Murugesan, S.; Kozlovskaya, V.; Zhang, R.; Velu, S. E.; Kharlampieva, E. Highly Efficient Delivery of Potent Anticancer Iminoquinone Derivative by Multilayer Hydrogel Cubes. *Acta Biomater.* **2017**, *58*, 386−398.

(66) (a) Liu, P.; Luo, Q.; Guan, Y.; Zhang, Y. Drug Release Kinetics from Monolayer Films of Glucose-Sensitive Microgel. *Polymer* **2010**, *51*, 2668−2675. (b) Sun, S.; Wu, P. A One-Step Strategy for Thermal- and pH-Responsive Graphene Oxide Interpenetrating Polymer Hydrogel Networks. *J. Mater. Chem.* **2011**, *21*, 4095−4097.

(67) (a) Hazlett, K. R. O.; Michalek, S. M.; Banas, J. A. Inactivation of the gbpA Gene of *Streptococcus mutans* Increases virulence and Promotes *In Vivo* Accumulation of Recombinations Between the Glucosyltransferase B and C Genes. *Infect. Immun.* **1998**, *66*, 2180−2185. (b) Michalek, S. M.; McGhee, J. R.; Shiota, T.; Devenyns, D. Virulence of *Streptococcus mutans*: Cariogenicity of *S. mutans* in Adult Gnotobiotic Rats. *Infect. Immun.* **1977**, *15*, 466−471.

(68) Keyes, P. H. Dental Caries in the Molar Teeth of Rats. II. A Method for Diagnosing and Scoring Several Types of Lesions Simultaneously. *J. Dent. Res.* **1958**, *37*, 1088−1099.

(69) Liu, C.; Worthington, R. J.; Melander, C.; Wu, H. A New Small Molecule Specifically Inhibits the Cariogenic Bacterium *Streptococcus mutans* in Multispecies Biofilms. *Antimicrob. Agents Chemother.* **2011**, *55*, 2679−2687.

(70) Zhang, Q.; Nguyen, T.; McMichael, M.; Velu, S. E.; Zou, J.; Zhou, X.; Wu, H. New Small-Molecule Inhibitors of Dihydrofolate Reductase Inhibit *Streptococcus mutans*. *Int. J. Antimicrob. Agents* **2015**, *46*, 174−182.

(71) (a) Lynch, D. J.; Michalek, S. M.; Zhu, M.; Drake, D.; Qian, F.; Banas, J. A. Cariogenicity of *Streptococcus mutans* Glucan-Binding Protein Deletion Mutants. *Oral Health Dent. Manage.* **2013**, *12*, 191−

https://doi.org/10.1021/acs.jmedchem.3c00272
J. Med. Chem. 2023, 66, 7909−7925

199. (b) Peng, X.; Zhang, Y.; Bai, G.; Zhou, X.; Wu, H. Cyclic di-AMP mediates biofilm formation. *Mol. Microbiol.* **2016**, *99*, 945−959.

https://doi.org/10.1021/acs.jmedchem.3c00272
J. Med. Chem. 2023, 66, 7909−7925